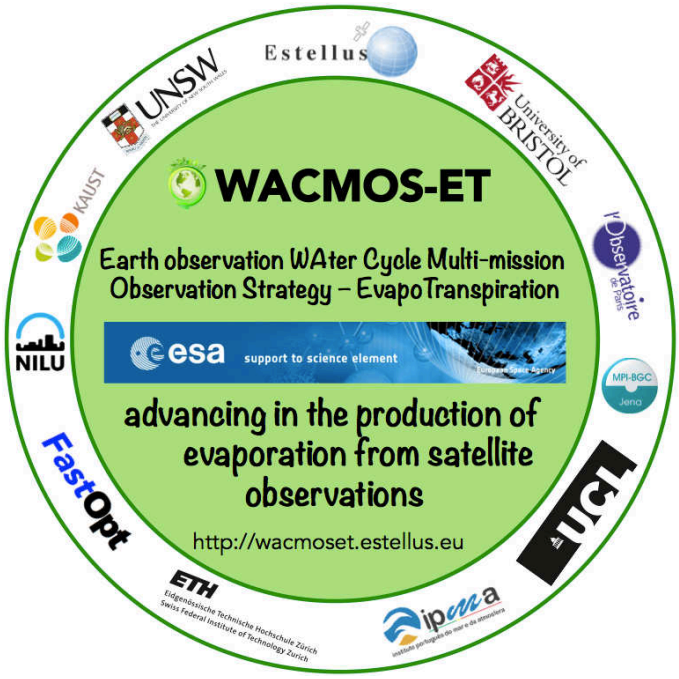

WP2230

fAPAR/LAI Product Validation Report

Prepared by:

Mat Disney

NCEO/Remote Sensing Group, Dept. of Geography, University College London, Gower Street, London WC1E 6BT, UK

Jan-Peter Muller, Said Kharbouche

Imaging Group, Mullard Space Science Laboratory, Dept. of Space and Climate Physics, University College London, Holmbury St Mary, RH5 6NT, UK

Thomas Kaminski, Michael Vossbeck

FastOpt, Lerchenstrasse, D-22767 Hamburg, Germany

1 LAI and fAPAR definitions

1.1 Leaf area index (LAI)

LAI, in an ecological sense, is (typically) defined as the total canopy area per unit ground area (m^2 m^{-2}) (Asner et al., 2003) and ranges from 0 (bare ground) to over 10 (dense forest). LAI determines the interception of solar energy (and thus the fraction of absorbed photosynthetically active radiation, fAPAR) for photosynthesis. LAI in a remote sensing sense by contrast, is defined as one-sided leaf area per unit ground area (m^2 m^{-2}) i.e. 0.5 of total (e.g. Chen & Black, 1992). There are various ways LAI has been considered in remote sensing and ecology, primarily via the projected surface area for light interception consideration; as half the total interception area, to account for non-flat (e.g. needle) shapes; as various functions of projected leaf area, considering common leaf angle distributions (Ross, 1981; Liang, 2004). Light is a directional resource that is greatest at the top of the canopy and decreases exponentially with depth through the canopy, the decrease being stronger with increasing projected leaf area.

Here, LAI is defined as: half the total canopy area per unit ground area (m^2 m^{-2}). This is consistent with the earth observation (EO)-derived products used here i.e. the WACMOS-ET product, derived from the JRC two-stream inversion package (hereafter, TIP – see view-source: http://fastopt.com/products/tip/tip.html) of Pinty et al. (2006; 2010a, b; 2011), as well as with the NASA MODIS LAI/fAPAR product (Knyazikhin et al., 1998, 1999; http://modis.gsfc.nasa.gov/data/atbd/atbd_mod15.pdf).

1.1.1 Caveats: LAI

Despite the (seemingly) relatively simple and physically-meaningful definition of LAI given above, two key issues must be considered in practice when using LAI derived from EO data.

Effective LAI and clumping

LAI can only be measured directly via destructive harvesting and scanning/weighing. Such measurements are hard to make over anything other than very small areas (few m^2) and are rarely carried out as a result. Indirect methods can be used to infer LAI, typically via optical methods such as hemiphotos, or using instruments that compare light levels above and below the canopy (LiCOR LAI2000, Sunscan). In these cases, LAI is inferred based on assumptions of the canopy absorption properties (e.g. all canopy elements are black, which is not the case in the visible/NIR) and architecture (e.g. assuming the canopy is horizontally homogeneous) e.g. see Joncheere et al. (2004) and Weiss et al. (2004).

To estimate LAI (and fAPAR) from EO data, surface fluxes, or albedos (e.g. visible and NIR albedo here) are used to invert a radiative transfer (RT) scheme that predicts these properties, with particular values of (among other parameters) LAI. Note that albedo values are not direct observations per se, but are model-derived values produced from angular samples of surface reflectance, interpolated over angle and time via RT model schemes (GlobAlbedo ATBD). A key requirement for retrieval of LAI should be that assumptions underlying the RT schemes used for both generating flux values and for LAI retrieval should be the same. However, this is rarely the case in practice. To achieve this, Pinty et al. (2006) suggest adopting an 'effective' LAI value $\widetilde{LAI}$ i.e. $\widetilde{LAI} = \langle LAI \rangle \zeta$ where <LAI> is the domain averaged LAI and ζ is a structural term that encapsulates the fact that real canopies are not turbid media but are clumped at multiple scales (cm's to 10's of m). Clumping acts to reduce

$\widetilde{LAI}$ compared to the true value, $\langle LAI \rangle$, as the degree of clumping increases. Regular canopies will have $\widetilde{LAI} > \langle LAI \rangle$ (Weiss et al., 2004).

The adoption of effective LAI permits a solution to the 1D limiting case of RT in a 3D canopy that is consistent with the assumptions made in many surface flux retrievals, as well as in large-scale Land Surface Models (e.g. see Widlowski et al., 2011). This assumption also allows the use of a relatively simple two-stream 1D RT scheme that can be applied to large (global) datasets. In this case, $\widetilde{LAI}$ is then an optical thickness. Crucially however, values of $\widetilde{LAI}$ are not the same as $\langle LAI \rangle$, which in turn are not the same as the LAI that would be measured on the ground (unless measured over some large, discrete canopy volume). That is, some of the resulting RT model parameters will be 'effective' parameters and will not have a direct (physically-defined, measurable) meaning. These effective parameters allow solution of the 1D RT problem by representing domain-averaged quantities that are forced to satisfy the constraints associated with a 1D representation of what is an inherently 3D system (Pinty et al., 2006).

We make this point to highlight the fact that care must be taken in comparing and interpreting LAI values derived from different sources: different assumptions will lead to different values of LAI. These assumptions should be made explicit in a particular model or application, so differences can be quantified and/or accounted for (e.g. via cross-calibration of LAI values). Here, LAI derived from the TIP is a 1D-equivalent LAI, for solving RT in a 3D medium and **IS** consistent with the fluxes from which it is derived. It is **NOT** consistent with LAI derived using a 3D RT scheme that allows some form of horizontal clumping (e.g. MODIS LAI), and will typically be lower than such a value. **NEITHER** of these values is directly comparable with values measured in the field using indirect, optical methods. **NONE** of these indirect estimates are directly comparable with direct, destructively-measured LAI. However, there is a high degree of correlation between these values, which can be locally calibrated, or generalised across biomes and scales (i.e. for a particular scale/type of clumping).

SCALE

The dimensionless LAI is normally well-correlated with fAPAR (especially in healthy, green vegetation), The effective LAI (LAI_e) is retrieved LAI assuming random distribution of leaves. The issue of clumping i.e. spatial aggregation across scales is illustrated in Figure **1**, which shows various vegetation canopies from a highly-simplified horizontally homogeneous case through to canopies with both horizontal and vertical clumping. The same total amount of leaf material (LAI) may be present in each case, but clearly the arrangement of the material (even in these simple cases) will determine the radiometric response (Widlowski et al., 2004). We see further in Figure **1** how the scale of observation alters the information available from a measurement at aggregation from 0.1m (~ leaf scale) to 30m (Landsat-like scale). Much if not all of the information on the spatial arrangement of the canopy has been lost, even down to the number of trees in the scene, yet the underlying 'real' LAI is the same. Liang (2002, 2004) demonstrates that the models which allow us to relate radiometric variables measured at one scale, to ecological (structural/radiometric) properties at a (usually) finer scale do not in general scale linearly across space, and nor should we expect them to. Recent work has considered the EO parameter scaling issue from an information content perspective.

The NASA MODIS LAI (and associated fAPAR) products are a good example of this (Knyazikhin et al., 1998), using a detailed biome-specific model of vegetation structure to simulate the radiometric response. These products in turn are used as the basis for the widely-

used MODIS-derived products related to carbon uptake i.e. net photosynthesis and gross primary productivity (Running et al., 1999).

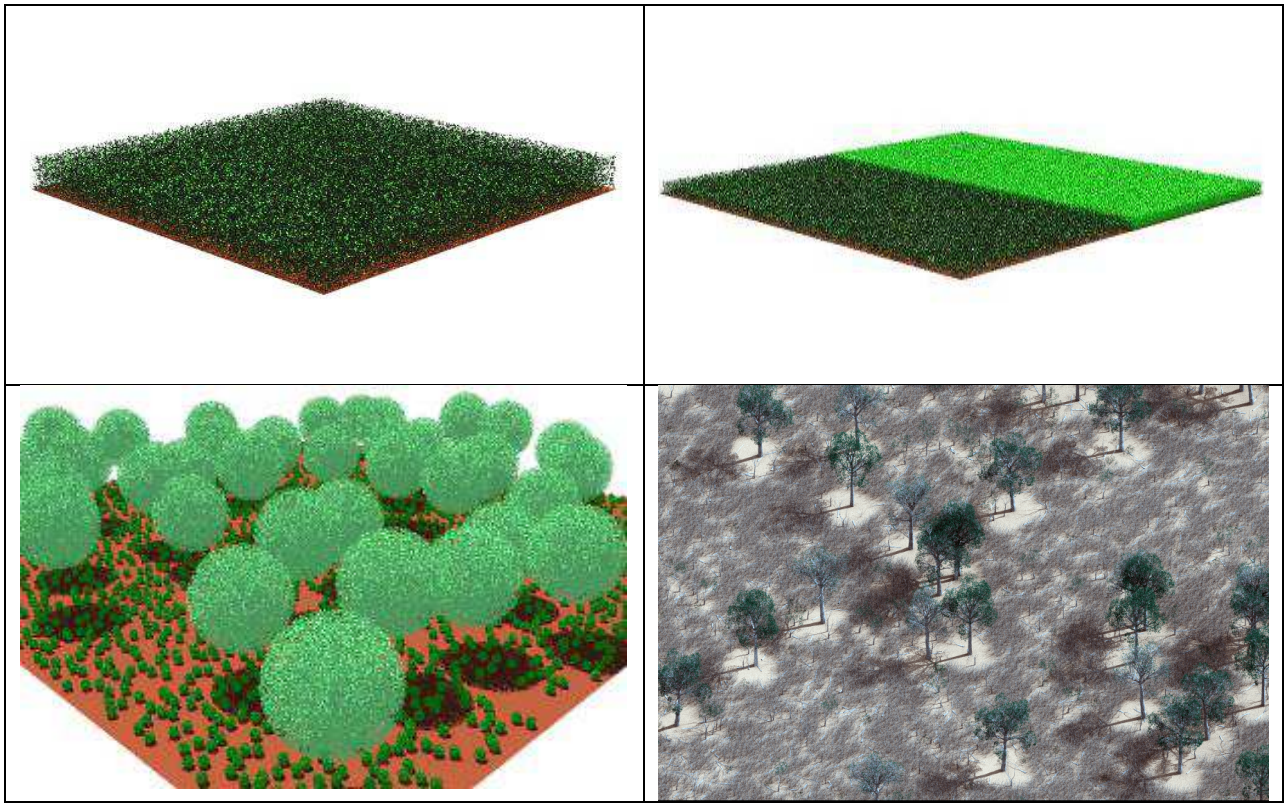

Figure 1 Spatial aggregation across scales shown in simplified vegetation canopies from a highly-simplified horizontally homogeneous case (top left: 1D approximation, top right: same as top left but leaf area arranged in two different densities) through to canopies with both horizontal and vertical clumping (bottom left: clumping at the overstory and understory level, bottom right: 3D model of a savannah canopy, 50m across). The same total amount of leaf material may be present in each case, but the arrangement of the material determines the radiometric response independently of the biochemical scattering properties of the leaves and soil. All images © RAMI initiative (http://rami-benchmark.jrc.ec.europa.eu/HTML/Home.php) except lower right (M. Disney). From Pfeifer et al. (2011).

1.2 fAPAR: fraction of absorbed photosynthetically active radiation

Here, fAPAR is defined as: the fraction of absorbed photosynthetically active radiation (PAR, 400-700 um). fAPAR is generally more straightforward to define than LAI, if not to measure. Here it is produced in a step subsequent to the LAI retrieval procedure. fAPAR is a dimensionless variable, varying between zero and one, and is related to the state and change of vegetation amount and productivity. Ceccherini et al. (2013) point out that due to the requirement for consistent radiometric processing, it is difficult to generate long time series of fAPAR observations due to inconsistencies between sensors and drifts in calibration of single sensors over time.

1.2.1 Caveats: fAPAR

Again, fAPAR would seem, in principle, to be an even more straightforward property to define and hence to use than LAI. However, as for LAI, fAPAR derived from a radiative transfer model inversion against EO data depends on the assumptions of the RT model. Again, the difference between a 1D and 3D approach will be perhaps the largest impact on derived fAPAR: that derived from a 1D RT model will not be directly comparable with that derived from a 3D model. In particular, magnitudes will likely be different.

In a recent discussion of satellite-derived biophysical parameters, Bojinski et al. (2014) discuss the issue of so-called Essential Climate Variables (ECVs) i.e. "physical, chemical or biological variable(s) or a group of linked variables that critically contribute to the characterization of the Earth's climate". They use fAPAR as an example ECV, pointing out that identifying fAPAR as an ECV has helped focus attention on retrieving fAPAR, resulting in multiple fAPAR datasets. They note that there is no single central definitive archive or product, nor has such been proposed. Ceccherini (2013) have proposed ways to generate consistent fAPAR records between fAPAR values derived from MERIS and SeaWIFS sensors. Figure **2** shows a comparison of 10-day composite fAPAR values derived from MERIS and SeaWIFS sensors from Ceccherini et al. (2013) over 2003. Although the agreement is generally close, there is some spread around the values even though these values are essentially calculated in the same way. Differences are likely due to differences in the outlier detection (cloud contamination), differences in sensor and illumination view angles, and existing biases in each dataset.

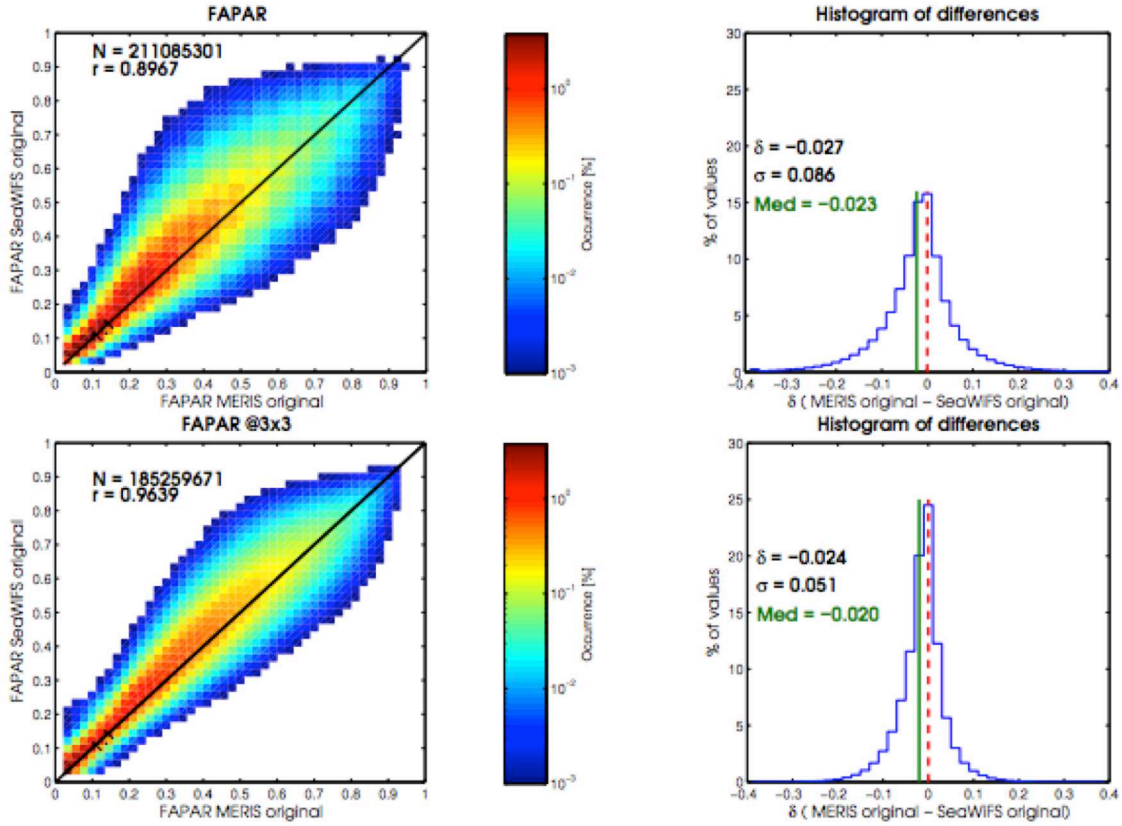

Figure 2 Comparison of fAPAR from two different optical sensors (MERIS and SeaWIFS), top for 1 x 1 pixel comparison and bottom for 3 x 3 pixel comparison. Red (blue) areas indicate higher (lower) density of sample points. From Ceccherini et al. (2013).

So, as for LAI, whilst the definitions of fAPAR are apparently clear and unambiguous, the resulting values derived from EO data are subject to the assumptions of the retrieval process and the characteristics of the observations from which they were derived.

1.3 Derivation of LAI and fAPAR: Summary of Algorithm

The products produced for the WACMOS-ET analysis are derived using the JRC Two Stream Inversion Package (JRC-TIP). The reader is referred to the series of papers describing

the RT theory and implementation of this package for full details (see view-source:http://fastopt.com/products/tip/tip.html and Pinty et al., 2007, 2010a and b). The underlying albedo data product generation is described on the project web-pages at http://www.GlobAlbedo.org and in detail in the GlobAlbedo Algorithm Theoretical Basis Document (GlobAlbedo ATBD, 2014). A brief overview is provided below.

1.3.1 Two-stream model

The TIP is an advanced inversion scheme explicitly developed for rapid, robust retrieval of surface variables (including LAI and fAPAR) from observations such as albedo, particularly at large spatial scales. In particular, the underlying radiation transfer (RT) model approach was designed to make use of so-called 'effective' parameters i.e. parameters that provide the correct radiation properties within the model, given the model assumptions, but parameters that would not be observed if they were (or could be) 'measured' in some way at the same scale as the model representing them (Pinty et al., 2006). Large-scale Earth system models (ESMs) almost always depend on a two-stream approximation to represent radiation fluxes at the surface; this in turn depends on a simplified 1-D approximation of surface canopy structural properties to be used in place of a more realistic 3-D representation. The approach of Pinty et al. (2006) is to accept this simplification, and use it as the basis of parameter retrieval, as long as the resulting parameters are then recognised as being the 'effective' 1-D equivalents required to provide a correct, consistent RT representation solution for what is an inherently 3-D canopy system. A key reason for taking this approach is that it is consistent with how radiation is treated in large-scale Earth System Models of climate and carbon cycle (Widlowski et al., 2011). A second reason for using this approach is that it is driven entirely by the underlying observations, unlike 3D model schemes which typically impose biome-specific prior structural information to separate grasses, deciduous and evergreen tree types for example.

The approach proposed by Pinty et al. (2006) uses a standard two-stream approach allowing decomposition of the directional hemispherical reflectance (DHR,) field emerging from the top of a canopy layer at depth z_{toc} into three terms:

$$R^{total}_{coupled}(z_{toc},\mu_0) = R^{Coll}_{veg}(z_{toc},\mu_0) + R^{UnColl}_{bgd}(z_{toc},\mu_0) + R^{Coll}_{bgd}(z_{toc},\mu_0)$$

Equation 1

where μ_0 is the solar zenith angle. The terms on the RHS represent, respectively: radiation that has interacted with the vegetation canopy elements only; that interacting with the soil only i.e. travelling both down and upwards through gaps in the canopy; and that interacting multiple times with both soil and background. The major advantage of this approach (over a more detailed 3-D approach for example) is that it can be solved analytically. The only additional requirement is the introduction of one additional parameter, a structural term representing the effects of spatial variation of leaf density. The use of effective variables guarantees the correct simulation of the scattered, transmitted and absorbed radiant fluxes. Pinty et al. (2006) derive values of the effective variables by inverting a 1-D radiant flux model against fluxes generated by a 3-D model. This guarantees accurate simulations of the three radiant fluxes when using, in direct mode, these effective values. In addition it does not require explicit consideration of other canopy elements (woody material) as these are considered implicitly in the diffuse (multiple scattered) fluxes. The resulting approach has been shown to agree very well with 3-D model simulations across a wide range of structural configurations (Pinty et al., 2006).

1.3.2 Two-stream model inversion

Inversion of the two-stream model is described in Pinty et al. (2007). In brief, the process is a standard inversion via the minimization of a cost function $J(\boldsymbol{X})$ of a vector of state variables (parameters) $\boldsymbol{X}$ that quantifies the difference between simulated, M(X), and observed, $\boldsymbol{d}$, of the fluxes plus the deviation of $\boldsymbol{X}$ from prior information on the state variables.

$$J(\boldsymbol{X}) = -\frac{1}{2}\Big[(M(\boldsymbol{X}) - \boldsymbol{d})^T \boldsymbol{C_d^{-1}} (M(\boldsymbol{X}) - \boldsymbol{d}) + \big(\boldsymbol{X} - \boldsymbol{X}_{prior}\big)^T \boldsymbol{C}_{\boldsymbol{X}_{prior}}^{-1} \big(\boldsymbol{X} - \boldsymbol{X}_{prior}\big)\Big]$$

Equation 2

The parameters $\boldsymbol{X}$ required by the two-stream radiative transfer model are LAI, leaf single-scattering albedo $\omega_l(\lambda_{1,2})$, background albedo $r_g(\lambda_{1,2})$ and $d_l(\lambda_{1,2})$ for the visible and near-infrared spectral domains respectively. By solving for the scattered and transmitted radiant fluxes, the absorbed component (fAPAR), or $A_{veg}^{Coll}(z_{bgd}, \mu_0)$ is given by considering energy closure in the case of a black (totally absorbing) background i.e. $A_{veg}^{Coll} = 1 - \big(R_{veg}^{Coll} + T_{veg}^{Coll}\big)$, where T_{veg}^{Coll} is simply the component transmitted by the vegetation through multiple interactions.

The model inversion problem is simplified by assumptions of observation and model parameter probability distribution as Gaussian, as well as a locally-linear approximation of $M(\boldsymbol{X})$. In this case, the posterior distribution of model parameters can be represented as

$$P(\boldsymbol{X}) \approx exp\left(-\frac{1}{2}\big(\boldsymbol{X} - \boldsymbol{X}_{post}\big)^T \boldsymbol{C}_{\boldsymbol{X}_{post}}^{-1} \big(\boldsymbol{X} - \boldsymbol{X}_{post}\big)\right)$$

Equation 3

where ^{T} represents the transpose operator; $\boldsymbol{X}_{post}$ and $\boldsymbol{C}_{\boldsymbol{X}_{post}}$ are the mean and covariance matrix of the maximum likelihood estimator of $P(\boldsymbol{X})$; $\boldsymbol{C}_{\boldsymbol{X}_{post}}^{-1}$ is the inverse of $\boldsymbol{C}_{\boldsymbol{X}_{post}}$. The $\boldsymbol{X}_{post}$ minimises a cost function $J(\boldsymbol{X})$In practice, J is minimized using a powerful gradient descent method. The required gradient is efficiently provided by the adjoint $J(\boldsymbol{X})$, Uncertainty ranges $\boldsymbol{C}_{\boldsymbol{X}_{post}}$ for $\boldsymbol{X}_{post}$ are approximated through inversion of the Hessian matrix of $J(\boldsymbol{X})$. of second partial derivatives. The Jacobian matrix of first derivatives of fluxes with respect to parameters is used to propagate parameter uncertainty to flux uncertainty. All derivative code is derived via automatic differentiation of the code that implements $J(\boldsymbol{X})$ **(**Voßbeck et al., 2008, 2011**)**.

Pinty et al. (2007) demonstrate the utility of the TIP in retrieving LAI and fAPAR from Moderate Resolution Imaging Spectroradiometer (MODIS) and Multiangle Imaging Spectroradiometer (MISR) broadband surface albedo products. More recently, Pinty et al. (2011, b) have demonstrated the performance of the TIP in deriving surface parameters on global scales from MODIS albedo data. In particular, they show the benefits of the TIP scheme for the generation of physically consistent information about the density and absorbing properties of the vegetation layer together with the brightness of the background underneath. LAI values follow expected trajectories of seasonal and spatial distributions. The estimated uncertainties on LAI are strongly correlated with the LAI itself and to a lesser extent to the brightness of the underlying background. In addition, the TIP allows control

over correlations between uncertainties of state variables of radiation transfer in the visible and near-infrared spectral ranges that are typically implicit in more approximate retrieval schemes based on empirical spectral indices.

In this project, the LAI and fAPAR values will be derived in the same way as outlined above, using the GlobAlbedo observations in the visible and NIR/SWIR.

1.4 Summary of WACMOS-ET provided LAI and fAPAR products

LAI and fAPAR are derived from an inversion of a 1D RT scheme (Pinty et al., 2010a, b) against the GlobAlbedo albedo values in the VIS (400-700 nm) and NIR/SWIR (700-3000 nm) wavelengths. The latter is referred to hereafter as the NIR channel for the avoidance of doubt. These values are consistent with the underlying observations, but are not those that would be obtained from a 3D RT inversion scheme (due to clumping), nor would they be those measured on the ground.

1.4.1 Spatial resolution

LAI and fAPAR data are produced at 3 separate resolutions: 1km, 5km and 25km. NOTE: the 5km and 25km data products are not simply aggregated versions of the 1km products, but are produced from up-scaled albedo data. These data in turn are calculated from up-scaled bidirectional reflectance factor (BRF) data. This is done in the GlobAlbedo processing to ensure energy conservation in upscaling albedo data at each of these native resolutions. Simple aggregation cannot account for sub-pixel heterogeneity correctly (due to non-linearities in spatial scaling) and so the products are generated using underlying albedo data at the native resolution.

1.4.2 Data format

Products are provided in the widely-supported NetCDF data format (http://www.unidata.ucar.edu/software/netcdf/) so –called Climate Format (netCDF(CF)). Data are stored on the MODIS SIN projection and the MODIS tiling system (http://modis-land.gsfc.nasa.gov/MODLAND_grid.html). There are 321 non-fill land tiles, each of 1200 × 1200 1km pixels (see below), 240 × 240 pixels at 5km and 48 × 48 at 25 km. The MODIS tiling system and the relevant tiles processed here are shown below in Figure **3**.

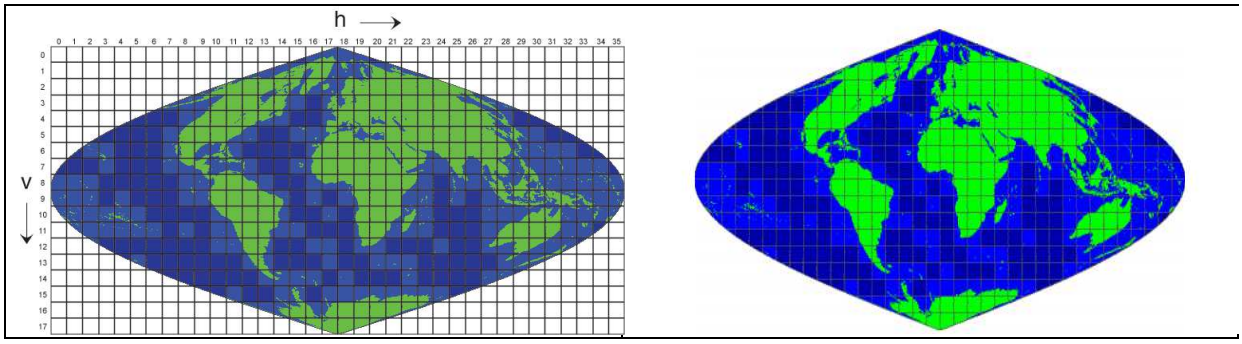

Figure 3 Left: MODIS tile map (from http://nsidc.org/data/modis/data_summaries/landgrid.html); right: non-fill land tiles in green (from GlobAlbedo ATBD, 2014)

1.4.3 Time period and data size

Products are generated for the years 2005-2007, globally, at each separate resolution. For 1 tile of either LAI or fAPAR, for 1 year at 1km the data size is ~439MB i.e. ~430GB unzipped for the global 3 year dataset; the 5km and 25km resolution datasets are ~13GB and ~600MB in total.

Snow-fraction areas are flagged in the processing during generation of the 1km GlobAlbedo data, and are flagged and processed as such in the 5km and 25km aggregated datasets (i.e. the aggregation of snow pixels is considered at those lower resolutions). This required special re-processing of the GlobAlbedo datasets.

2 Example LAI and fAPAR data

Figures below show examples of the global retrievals of LAI and fAPAR for day of year (DOY) 186, at 25 km resolution. Also shown are the retrieval uncertainties in each case.

2.1 Global LAI: 2006 DAY 185

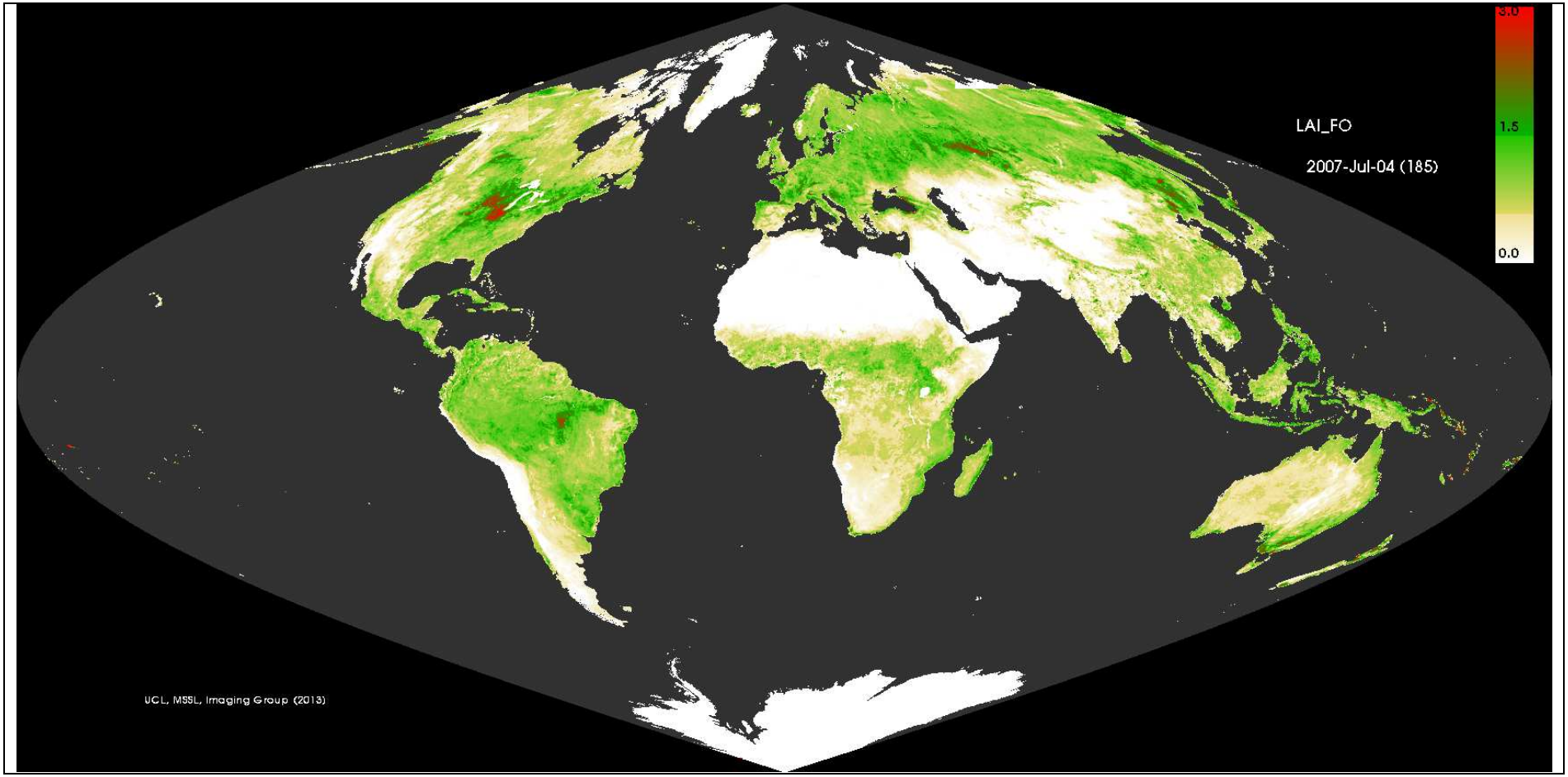

Figure 4 Global 25km resolution map of LAI (effective), for day of year 185 2006. Maximum LAI is around 3

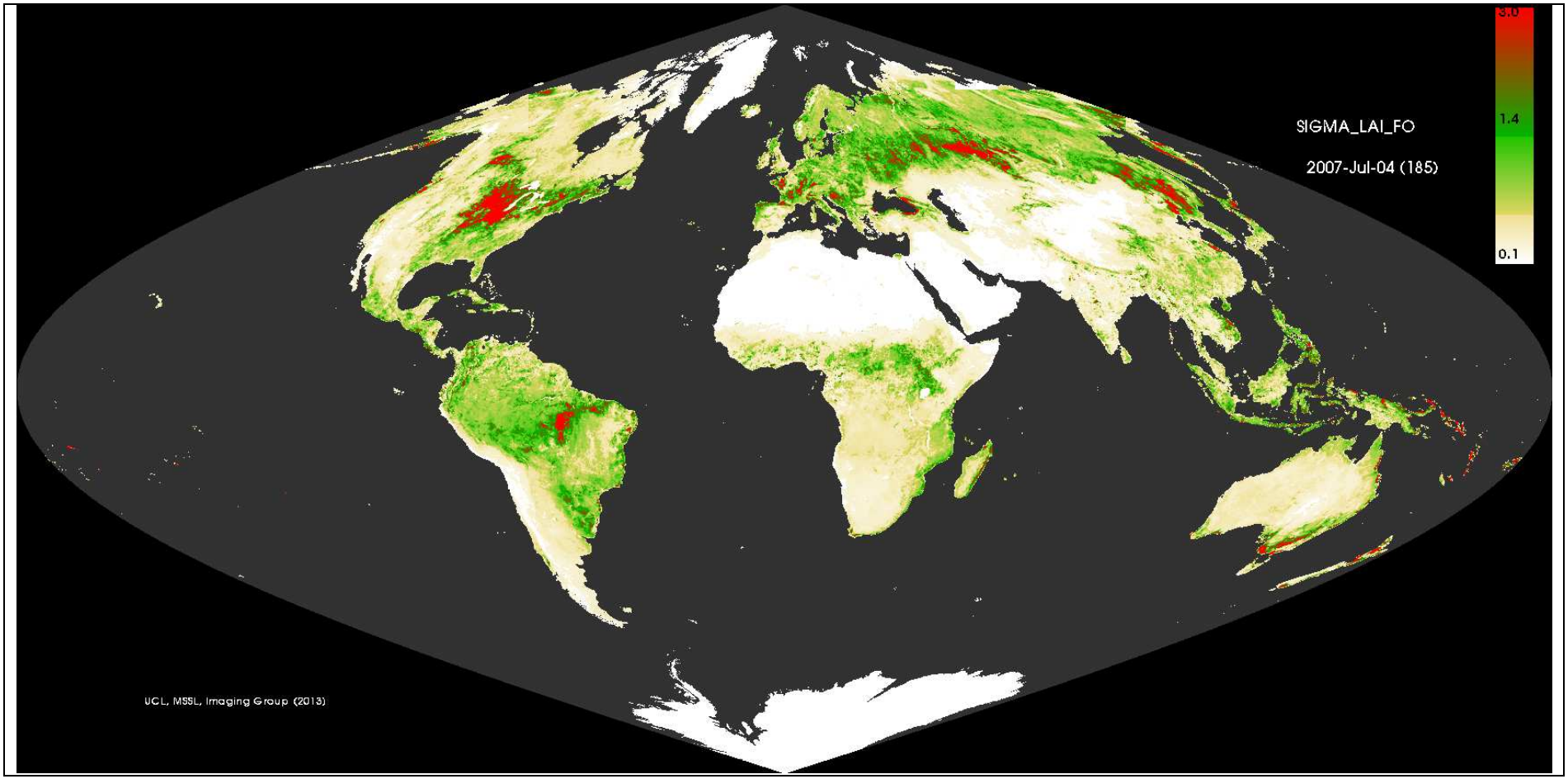

Figure 5 Global 25km resolution map of the uncertainty σ_{LAI} of retrieved LAI, for day of year 185 2006.

2.2 Global fAPAR: 2006 DAY 185

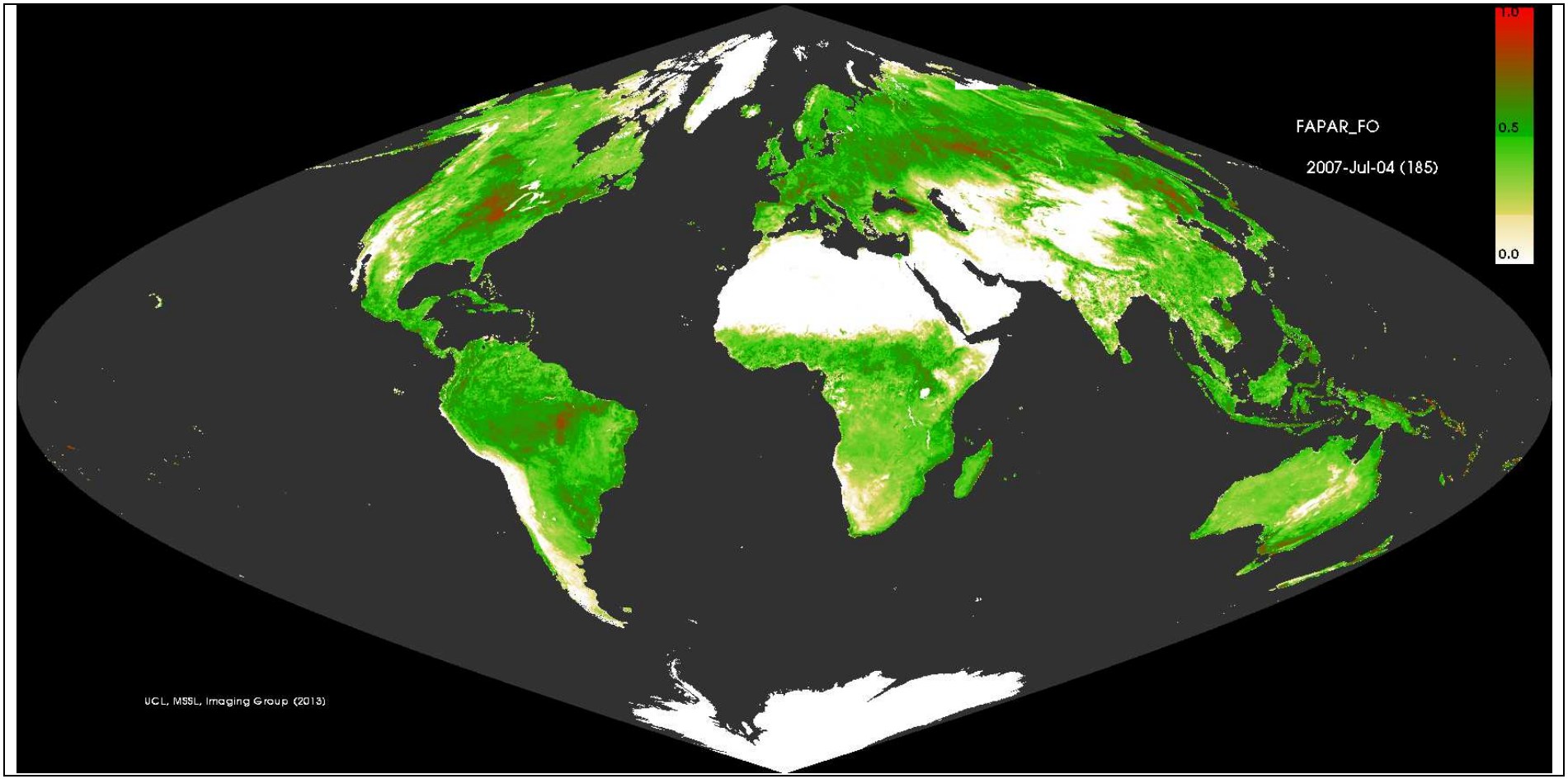

Figure 6 Global 25km resolution map of fAPAR, for day of year 185 2006.

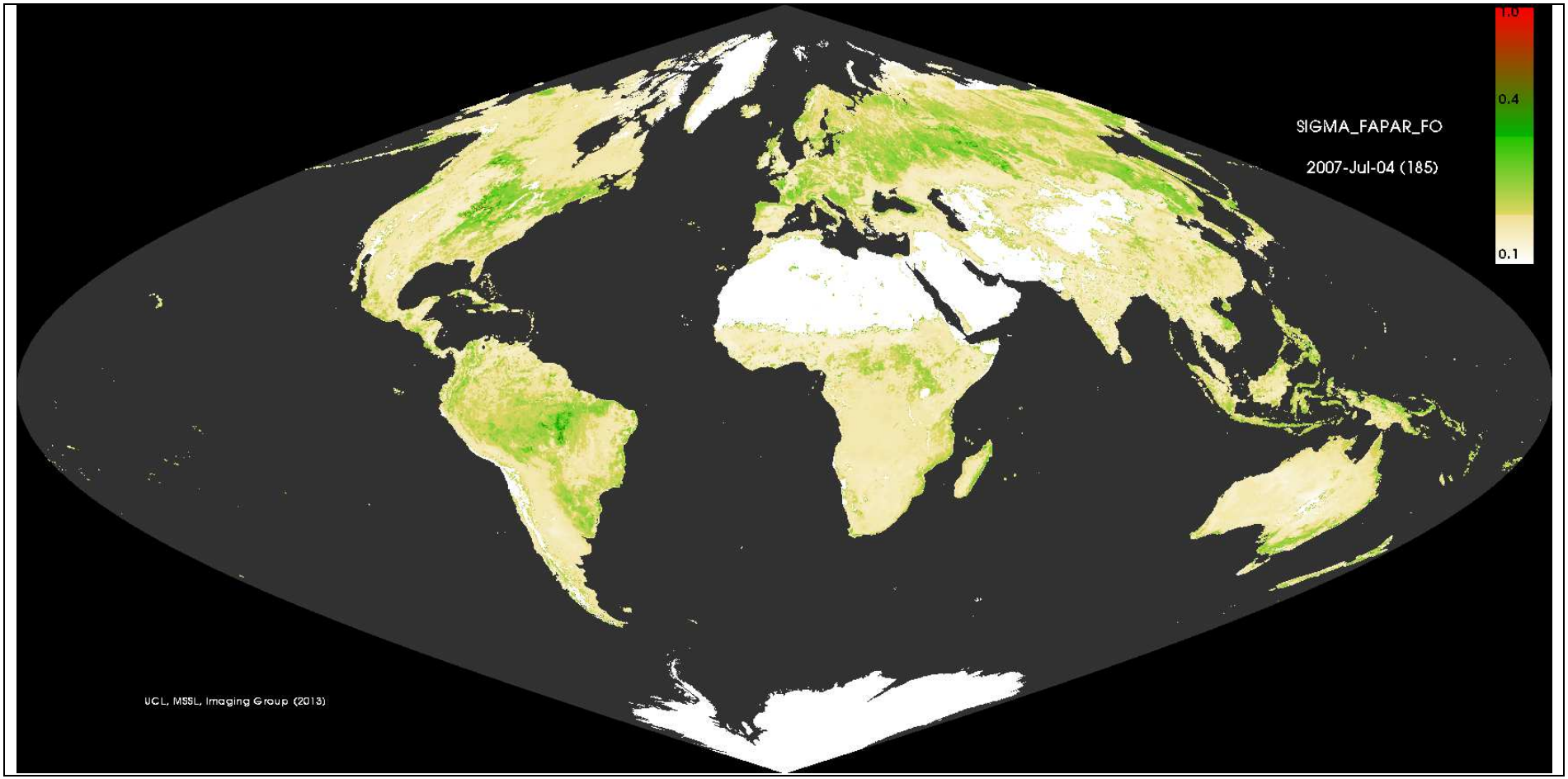

Figure 7 Global 25km resolution map of the uncertainty σ_{fAPAR} of retrieved fAPAR, for day of year 185 2006.

3 Comparison with MODIS LAI and fAPAR products

Here we show site and region comparisons with the MODIS LAI and fAPAR products, to illustrate consistency as well as differences with the products derived from the GlobAlbedo data using the JRC-TIP retrievals (referred to as TIP products below). An important point to note is that the MODIS LAI and fAPAR products are derived using different assumptions from those derived here; namely, the MODIS products use a biome-specific 3D solution of RT in the vegetation canopy (Knyazikhin et al., 1998, 1999). Choice of biome allows for clumping, among other aspects (such as cover and vegetation thickness). However, this means the two datasets are not directly comparable as described above. Comparisons are provided here as these are indicative of spatial and temporal consistency, rather than absolute accuracy or bias. The MODIS data used here for comparison are the MCD15A2 (https://lpdaac.usgs.gov/products/modis_products_table/mcd15a2) and MCD15A3 (https://lpdaac.usgs.gov/products/modis_products_table/mcd15a3) products, representing the MODIS combined Terra and Aqua instrument products, derived from 8-day (MCD15A2) and 4-day (MCD15A3) 1km composites of observations respectively. It is important to note that we do not imply that either product is 'right'; as described above, each product uses different assumptions, and these are different from those used in field measurements using optical devices, which are in turn not the same as direct, destructive measurements (the only real answer).

Comparisons are presented for specific flux tower sites, regionally over whole tiles, and finally, for whole-hemisphere seasonal comparisons.

3.1 Site comparisons

Separate site-level comparisons are shown below, for varying cover types across the US and Europe. Sites are chosen from the FLUXNET database (http://www.fluxdata.org:8080/SitePages/), where sites are well-characterised and studied over significant time periods.

An interface to the TIP LAI and fAPAR products through the GlobAlbedo website (see http://www.globalbedo.org/point_faparlai.php) is provided. The user can specify a site location (lat, lon) or MODIS tile location (horizontal and vertical tile ID, and sample and line within the tile) along with a region surrounding this pixel (from 1 x 1 km to 25 x 25 km), and a date range from any given Day_of_Year to any other DoY (within the 2005-2007 range). This will query the original data, generate text file output, plot the corresponding time series and scatter plot of TIP LAI and fAPAR against the corresponding MODIS 4 or 8-day LAI, fAPAR products and email the user with links to URLs with the results.

For each time series of observations, the TIP and MODIS values are plotted, as well as the uncertainty (σ) of the TIP retrievals. The uncertainty values are a by-product of the inversion process and are a true representation of the uncertainty in the underlying observations and retrieval process. Well-characterised uncertainty is a key advantage of the TIP process, depending as it does only on the observations themselves. Retrievals that require a priori model and retrieval assumptions may have more detailed representations of the canopy (e.g. 3D RT model approaches), but at the expense of assigning realistic uncertainty values to retrievals. This is due to the difficulty of assessing the contribution to uncertainty of a priori assumptions (e.g. biome choice, model structure) and how the uncertainty in underlying reflectance data feed through. In the MODIS LAI and fAPAR retrievals for example, there is an imposed band- and biome-specific threshold on allowable discrepancies between RT-

model simulated and MODIS surface reflectances, (see http://landweb.nascom.nasa.gov/QA_WWW/forPage/C005_Changes_LAI_FPAR.pdf). As a result uncertainty estimates are both constrained and quantised, and hence probably unrealistic. These values are not shown; this does not mean uncertainty is zero, but we have no basis for assessing the quality of these values, unlike the TIP uncertainty values.

3.1.1 ARM Southern Great Plains-Lamont, US

The ARM Southern Great Plains site, is situated in Lamont, Oklahoma, and is a cropland site (see http://www.fluxdata.org:8080/SitePages/siteInfo.aspx?US-ARM), with a generally low LAI in comparison to forest sites.

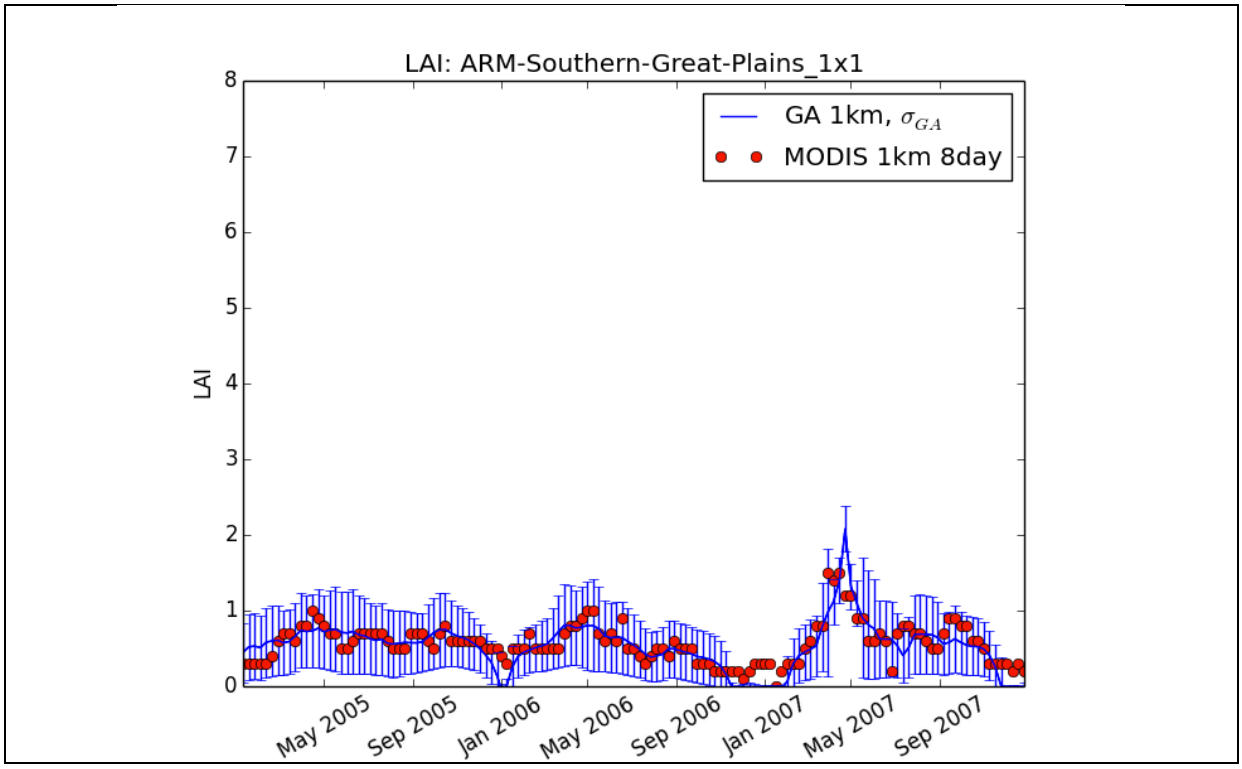

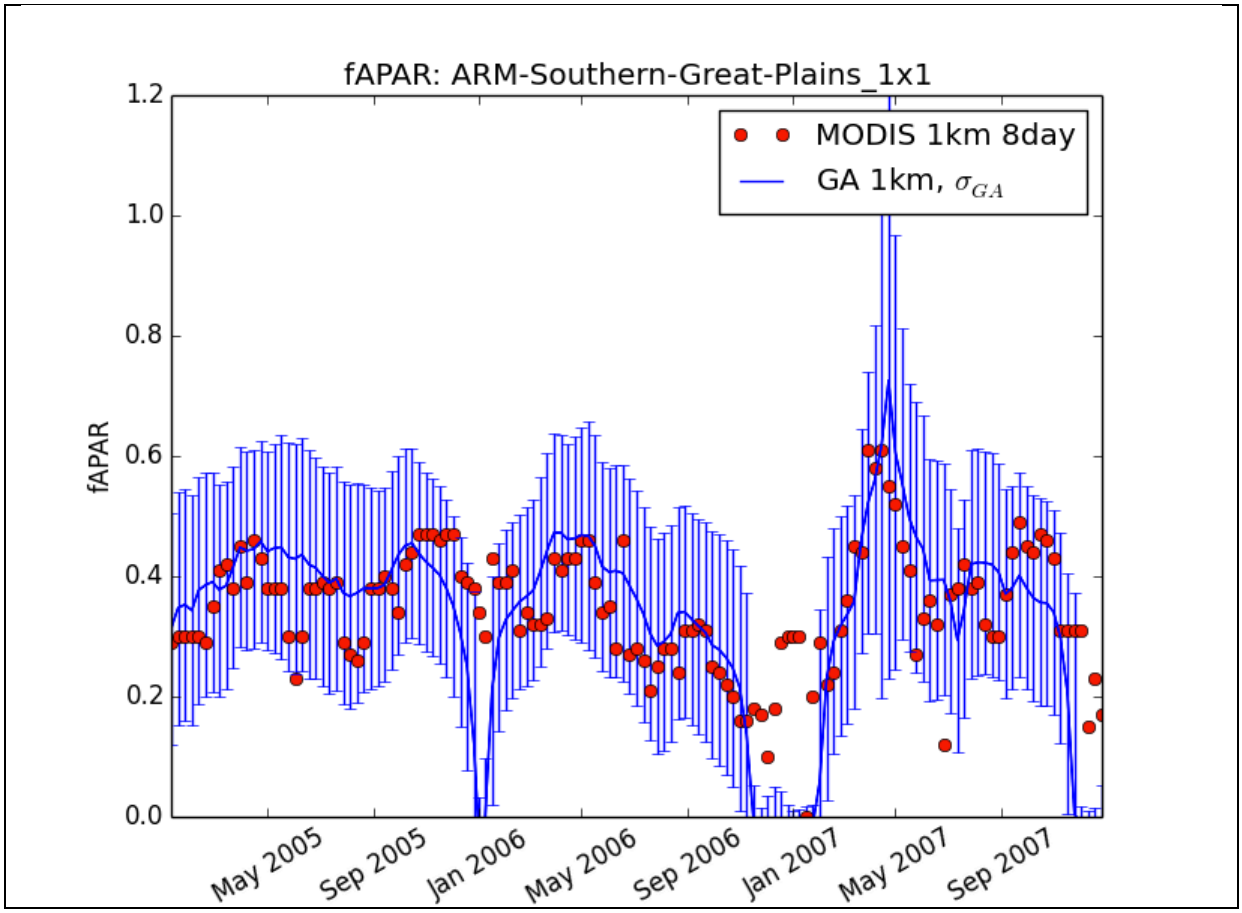

Figure 8 Comparison between JRC-TIP (blue) and MODIS 4 and 8-day (green, red) LAI (top) and fAPAR (bottom) over 2005-2007. Error bars for the TIP are 1 standard deviation of retrievals.

From the plots above it can be seen that both the magnitude and timing (phenology) of the TIP and MODIS products agree closely, particularly in LAI, with the TIP LAI generally more stable than the MODIS values. This is reflected in the scatter of the LAI and fAPAR shown below where the agreement between both datasets is quite high. The issue of clumping is likely to affect cropland sites such as this less than forest sites; at large scales croplands are relatively homogeneous, short-stature canopies with only row clumping due to the planting patterns. These variations will effectively disappear at the km-scale. The MODIS values fall within the TIP uncertainty ranges in all cases for LAI and for fAPAR in all cases bar observations at the start/end of each year, when retrievals are likely to be poor due to cloud and snow. Interestingly, the LAI and fAPAR for TIP drops to zero at these times, as might be expected, while the MODIS values can remain quite high.

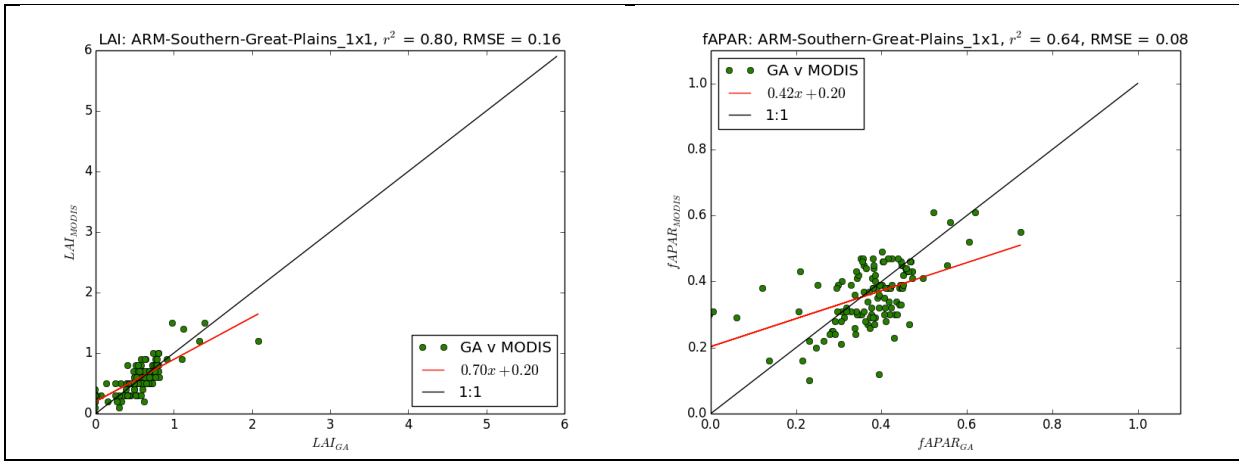

Figure 9 Scatter plots of comparisons shown above.

3.1.2 Hainich, Germany

Hainich is a deciduous broadleaf site 110km west of Jena, and is a mixed deciduous beech forest, unmanaged and at late stage of succession (see http://www.fluxdata.org:8080/SitePages/siteInfo.aspx?DE-Hai). It was also discussed in detail by Pinty et al. (2011)

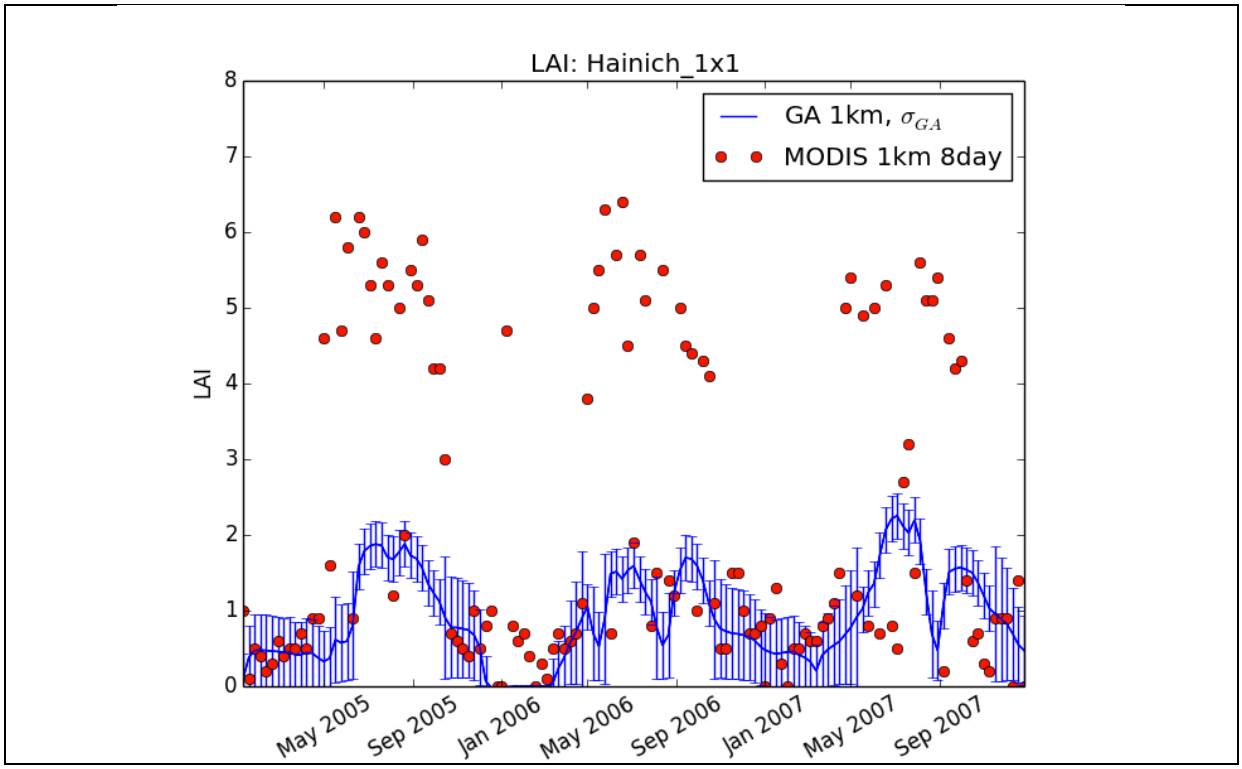

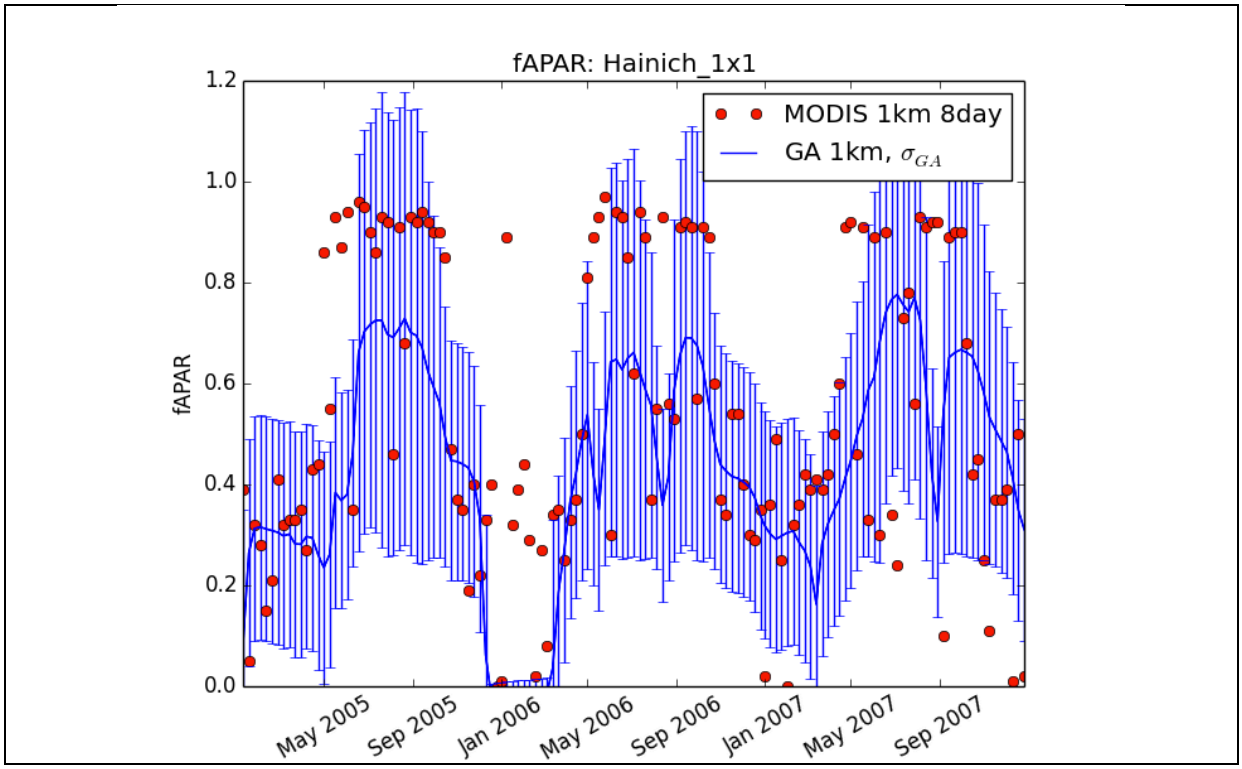

Figure 10 Comparison between JRC-TIP (blue) and MODIS 4 and 8-day (green, red) LAI (top) and fAPAR (bottom) over 2005-2007. Error bars for the TIP are 1 standard deviation of retrievals.

Here, we can see the issue of clumping reducing the TIP LAI and fAPAR below those derived from MODIS i.e. LAI varies from 0.5-2 over the season in the TIP data, and 0.5-6 in the MODIS data. Clumping is a far greater issue in a mixed deciduous woodland region of this sort. fAPAR tends to be 0.2 lower at the peak in the TIP compared to MODIS. A further feature of note is the dramatically increased stability of the TIP products compared to the MODIS values, which can vary by a factor of > 4 from week to week. This is likely due to cloud coverage in the underlying reflectance data from which the MODIS LAI and fAPAR products are derived, as well as transient snow cover that may get through the pre-processing stages contaminating RT model retrievals. This is much reduced in the GlobAlbedo data, which of course are model-derived angular integrals of directional surface reflectance, where the model is robust to outlier values in the input reflectance data (the angular model gives a prior expectation of surface angular reflectance behaviour).

For the LAI the MODIS values at peak season like well outside the uncertainty range of the TIP values; for the fAPAR this is rarely the case. The uncertainty of the TIP fAPAR is quite high across the season, likely due to the relatively sparse number of observations (clouds). As for the comparisons shown below, the apparent low correlation between the products in the scatter plots is almost all due to the week-to-week variation in the MODIS data.

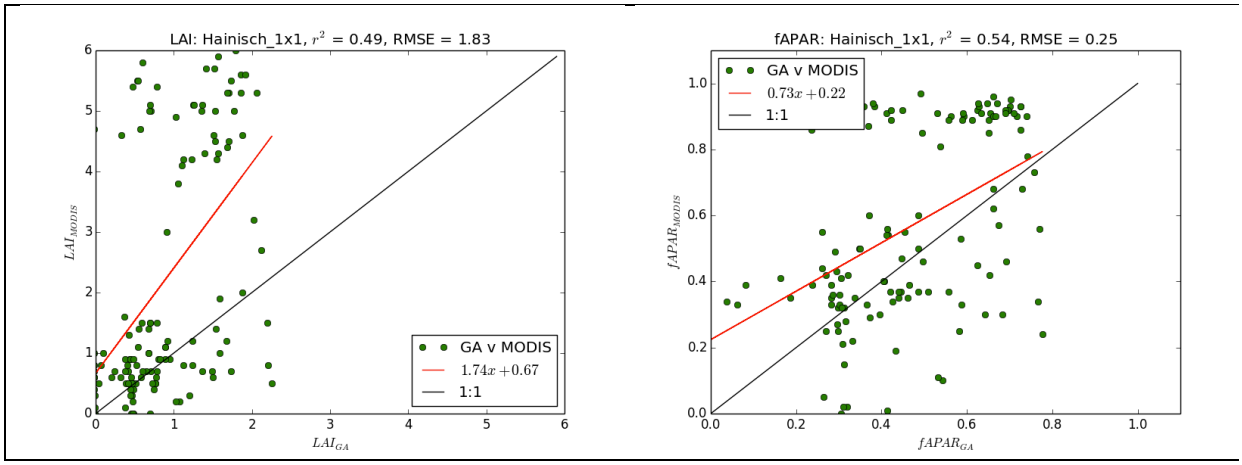

Figure 11 Scatter plots of comparisons shown above.

A further feature of note is the timing – the MODIS LAI tends to respond much earlier in the year to the rise in LAI, with the TIP values following up to 40 days behind in the case of 2005 and 2007. This is possibly due to the presence of understory. The MODIS retrievals are based on characterisations of the regions into one of 8 biome types, and RT model inversion includes the concept of an understory contribution as part of the background in the forest biome classes. The TIP retrievals from the GlobAlbedo data by contrast, make no assumptions about cover type and simply use the values of the input albedo. In an area where there is understory with a different phenology from the overstory (but both are green vegetation), the MODIS algorithm has the additional freedom to converge on a solution that may be a response to understory change, whereas the integrated albedo may change more slowly/smoothly than the underlying reflectance data.

3.1.3 Tharandt, Germany

Tharandt, Germany is an evergreen needleleaf site situated in the Saxony region (see http://www.fluxdata.org:8080/SitePages/siteInfo.aspx?DE-Tha).

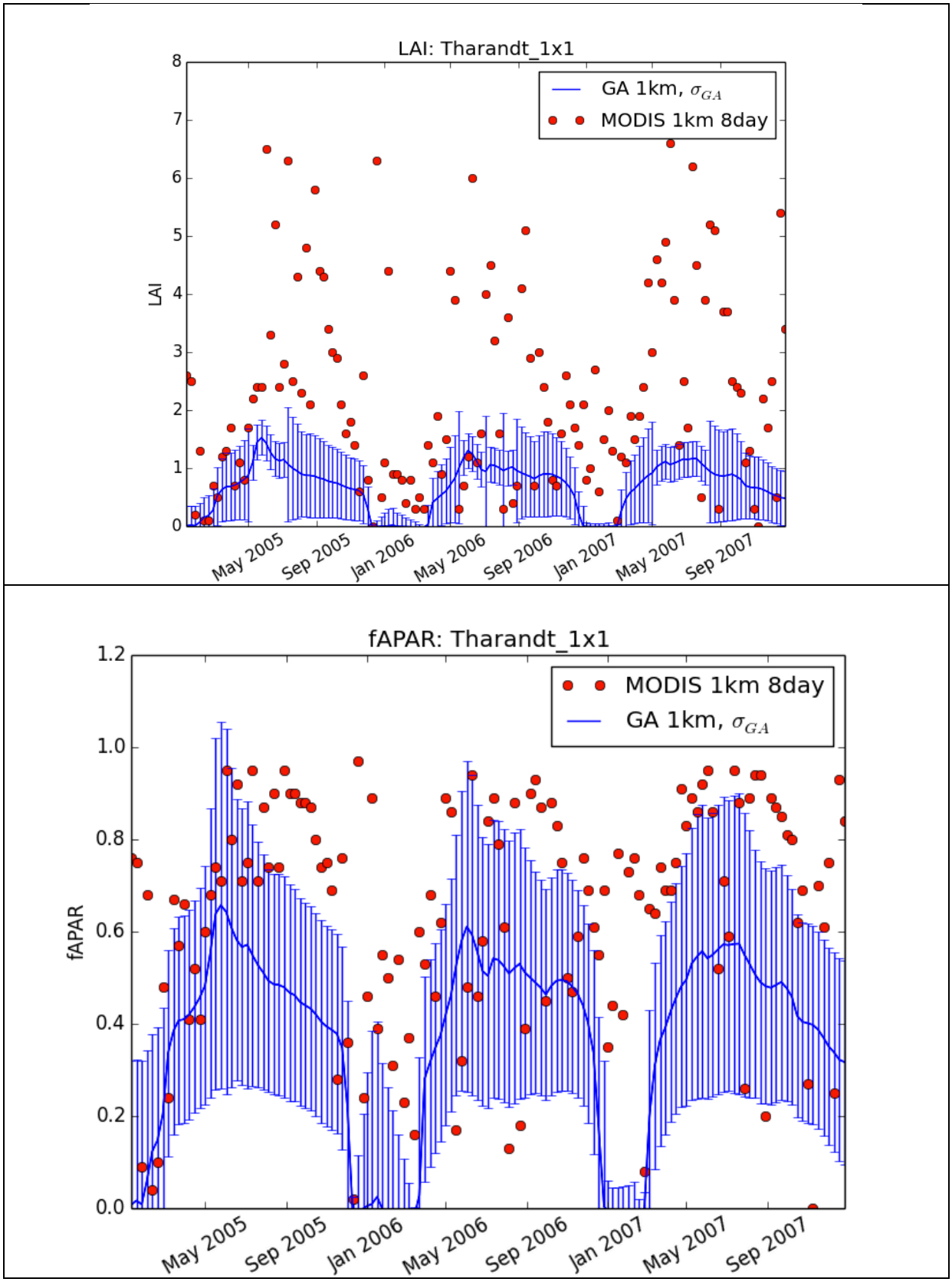

Figure 12 Comparison between JRC-TIP (blue) and MODIS 4 and 8-day (green, red) LAI (top) and fAPAR (bottom) over 2005-2007. Error bars for the TIP are 1 standard deviation of retrievals.

Here, in an evergreen needleleaf site, there is still an appreciable seasonal variation in LAI and fAPAR, in part due to understory, but also likely due to the green flushing of new needles in the spring of each year. Here, the TIP and MODIS-derived LAI and fAPAR are

much closer in timing of green-up and senescence. There is the same difference in lower peak LAI and fAPAR in the TIP cases than the MODIS values as seen in the Hainich case above, with an even greater difference in the peak values (up to 5 in some cases). Again, as seen above, most of the MODIS LAI values lie outside the TIP uncertainty ranges for much of the time, largely due to the very large variation in the MODIS data. Conversely, the majority of MODIS fAPAR values lie within the TIP uncertainty range.

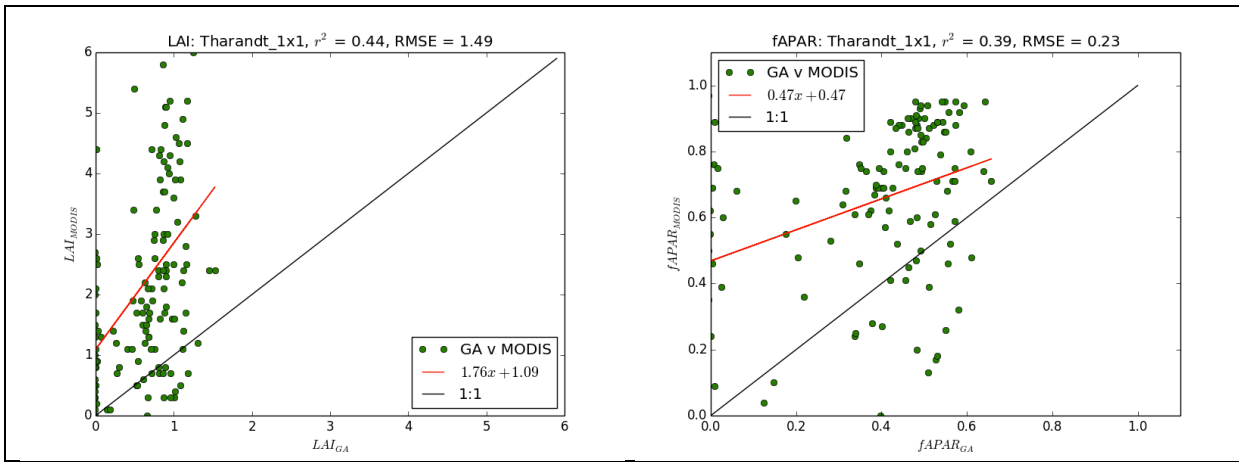

Figure 13 Scatter plots of comparisons shown above.

The peak fAPAR values differ by around 0.2 again, as above. This relatively large difference is reflected in the r^2 values of 0.44 and 0.39 for the LAI and fAPAR respectively. Again, the temporal variation of the TIP-derived products is much smaller than that from MODIS.

3.1.4 University of Michigan Biological Site, US

The UMBS site is located within a protected forest owned by the University of Michigan (see http://www.fluxdata.org:8080/SitePages/siteInfo.aspx?IT-Lec). The site is mixed mid-aged northern hardwoods, conifer understory, aspen, and old growth hemlock.

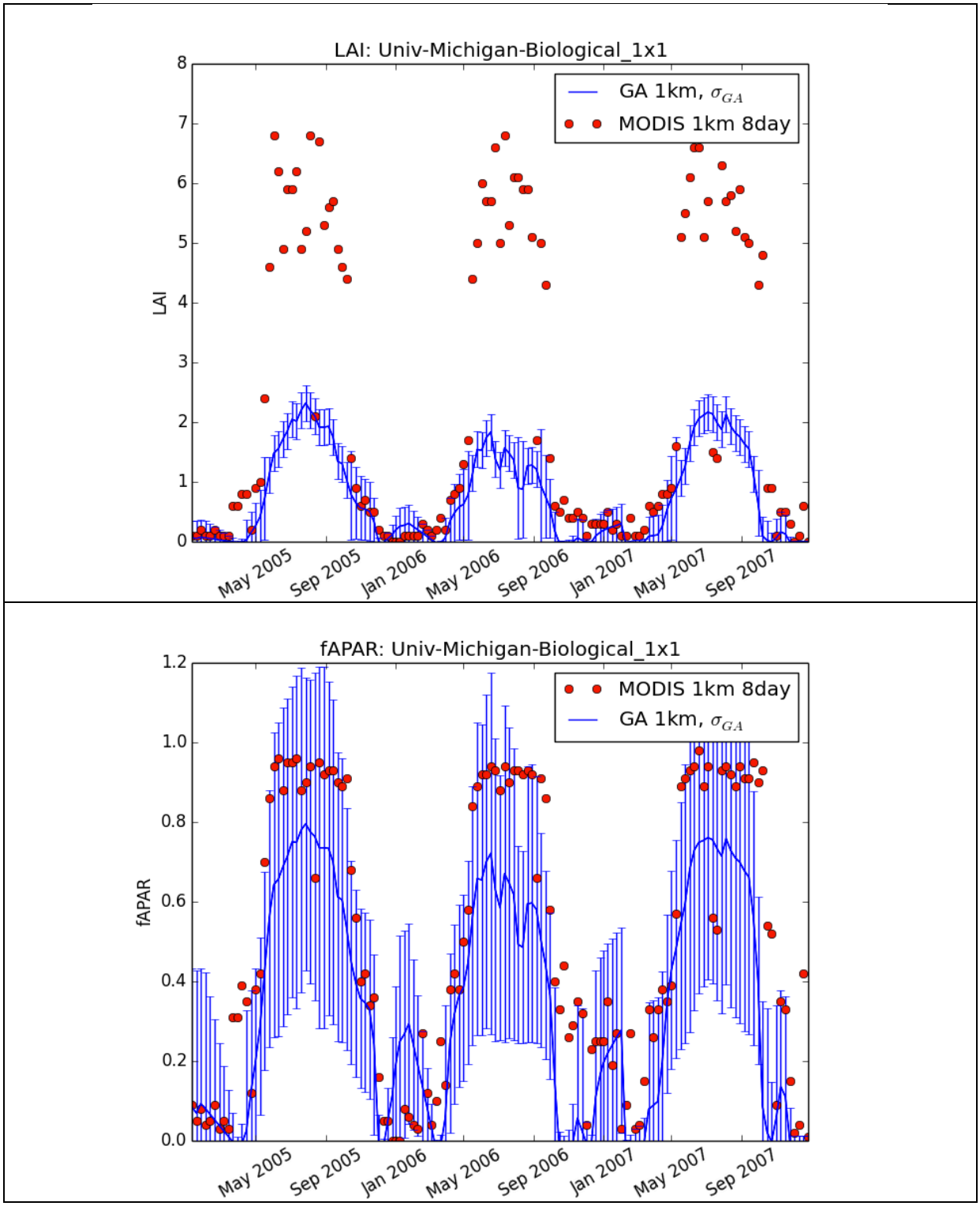

Figure 14 Comparison between JRC-TIP (blue) and MODIS 4 and 8-day (green, red) LAI (top) and fAPAR (bottom) over 2005-2007. Error bars for the TIP are 1 standard deviation of retrievals.

The seasonal variation for the MODIS LAI and fAPAR is in quite close agreement here, with the TIP LAI and fAPAR lagging the MODIS slightly. The magnitude of TIP LAI is again lower than MODIS, by a factor of ~3 at the peak. The difference in fAPAR is smaller this time, and very consistent at ~0.1 at the peak. This relatively close agreement is shown in the scatter plots below. The LAI values from MODIS are more realistic during the winter periods

here, close to zero. MODIS fAPAR values almost all lie within the TIP uncertainty ranges, except for a few winter periods.

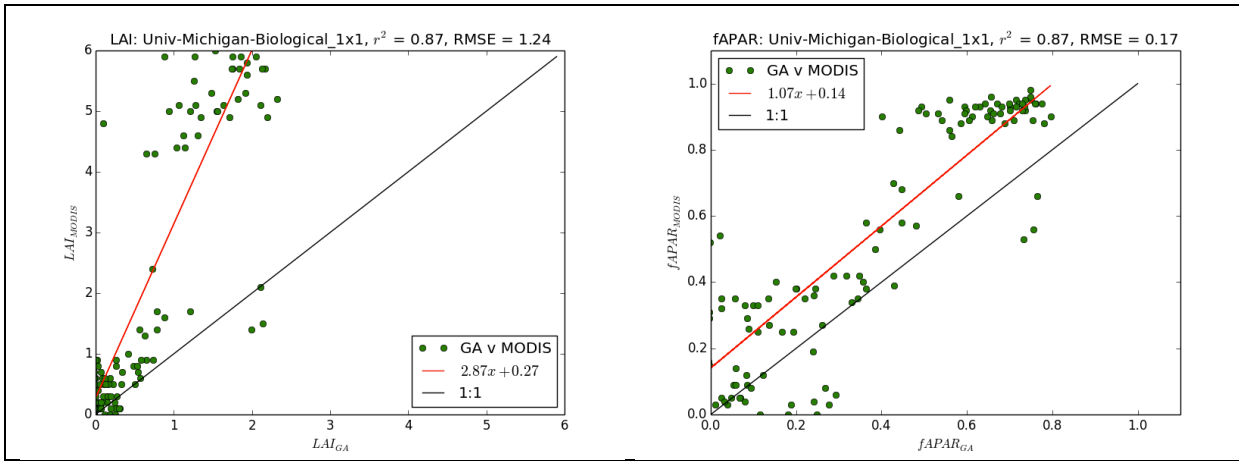

Figure 15 Scatter plots of comparisons shown above.

The scatter plots above show high correlations for both LAI and fAPAR. The gain of LAI to convert the TIP values to MODIS values is ~2.9. For fAPAR there is almost no gain required, and the offset is around 0.14.

3.1.5 El Saler, Spain

El Saler is a natural parkland evergreen needleleaf site, 20 km south of Valencia in southern Spain (see http://www.fluxdata.org:8080/SitePages/siteInfo.aspx?ES-ES1).

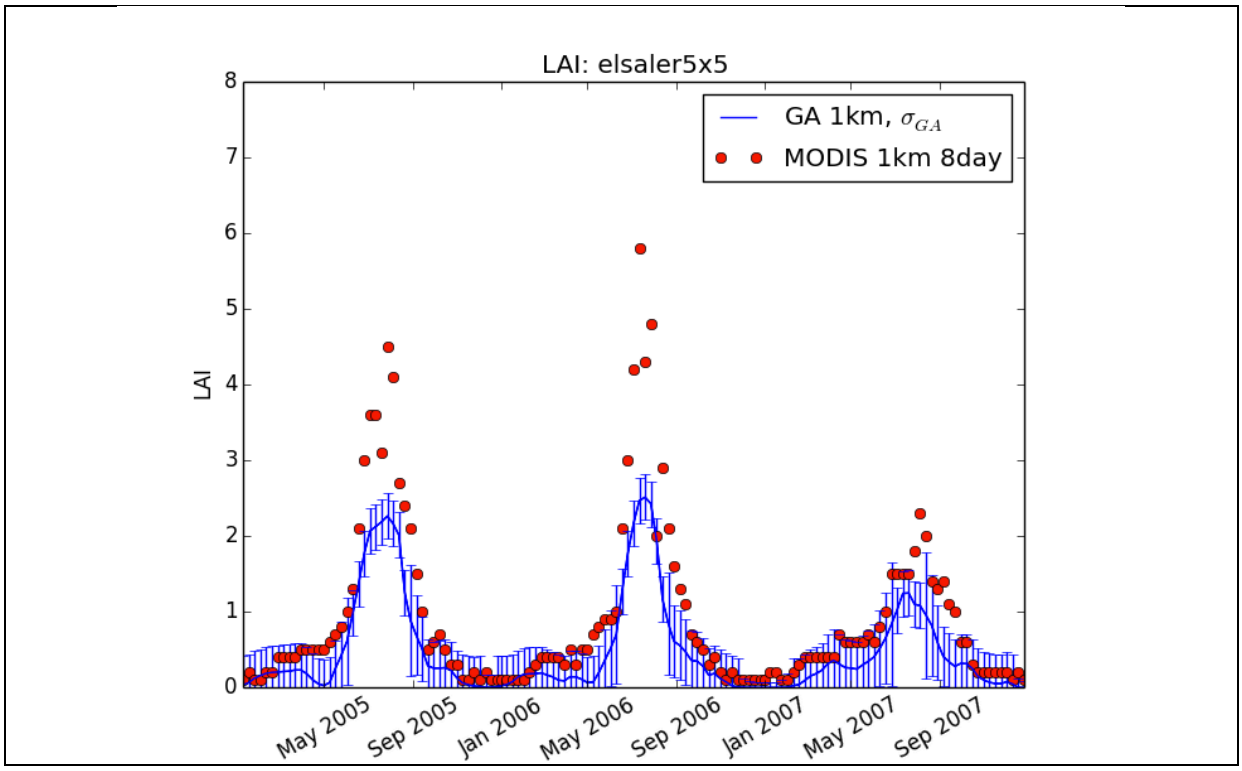

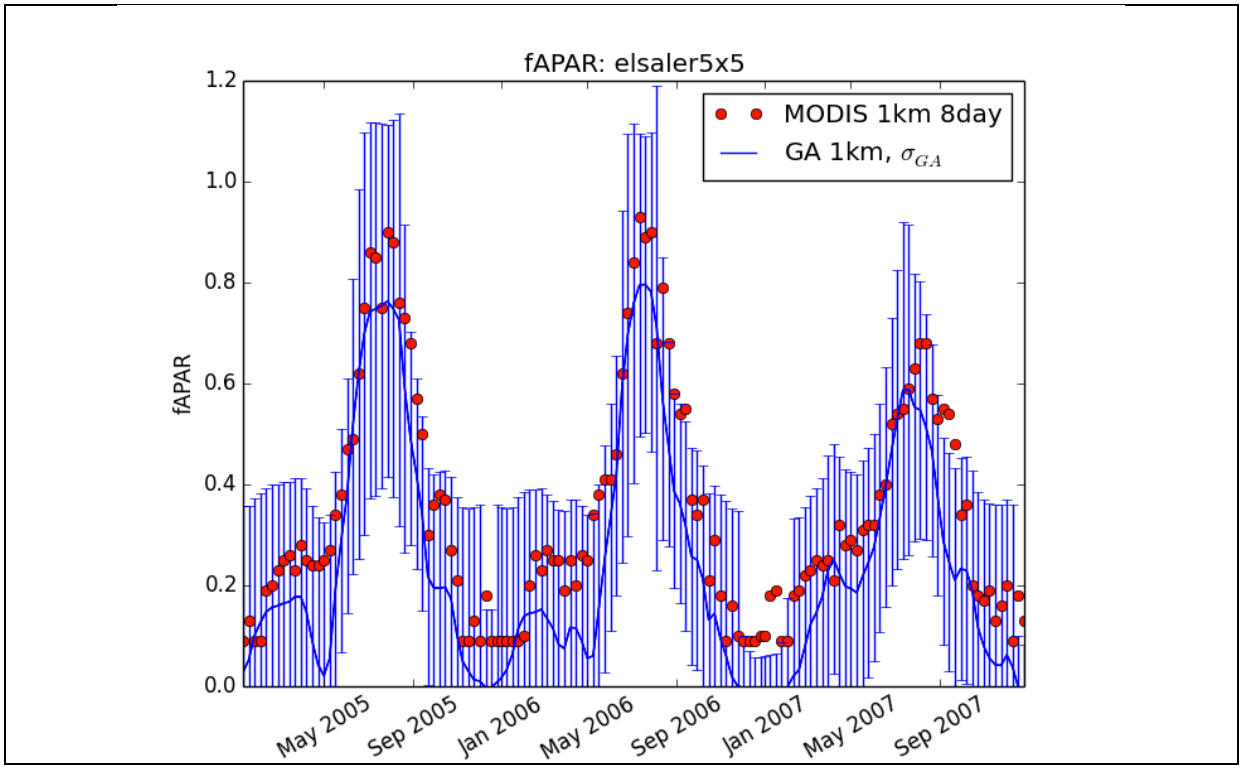

Figure 16 Comparison between JRC-TIP (blue) and MODIS 4 and 8-day (green, red) LAI (top) and fAPAR (bottom) over 2005-2007. Error bars for the TIP are 1 standard deviation of retrievals.

There is generally close agreement between the TIP and MODIS products at this site, both in terms of timing and magnitude. The peak LAI values are around a factor of 2 higher in the MODIS here; fAPAR values are within 0.1 or less. While the TIP values start from a lower baseline value in general, the green-up and senescence match that from MODIS quite closely, suggesting the signal is dominated by an obvious overstory canopy. The TIP uncertainty values for LAI are low through the year, suggesting the observations are generally of good quality.

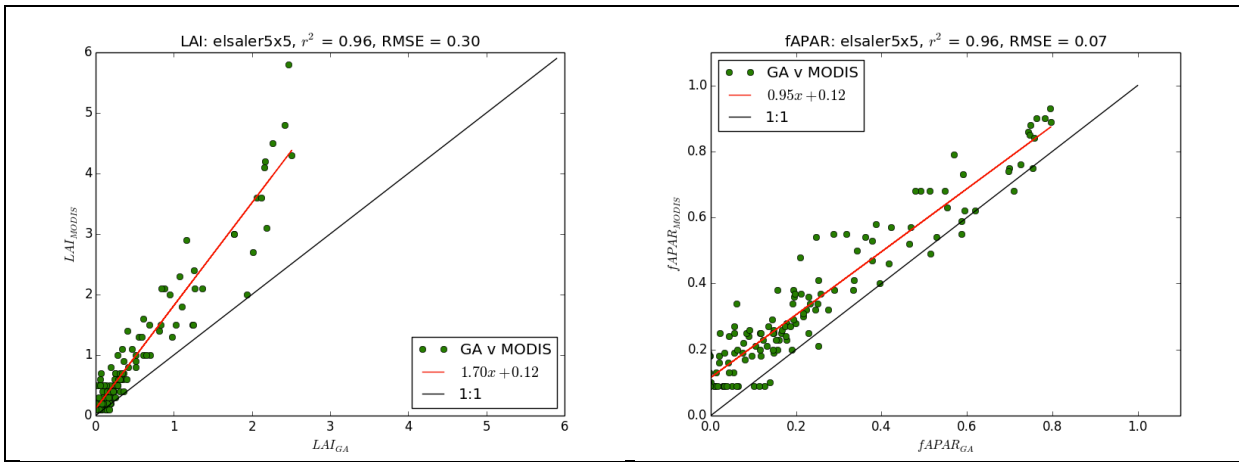

Figure 17 Scatter plots of comparisons shown above.

In this case, there is close agreement in timing and relative variation in magnitude. This is seen in the scatter of values, where the offset is relatively consistent i.e. the MODIS LAI is ~1.7 that of the TIP values. For the fAPAR there is very close agreement, with little difference in slope and an offset of 0.7.

3.1.6 Groundhog River, Canada

Groundhog River (FCRN or CCP site "ON-OMW") is situated in a boreal mixed forest in northeastern Ontario about 80 km southwest of Timmins near the Groundhog River (see http://www.fluxdata.org:8080/SitePages/siteInfo.aspx?CA-Gro).

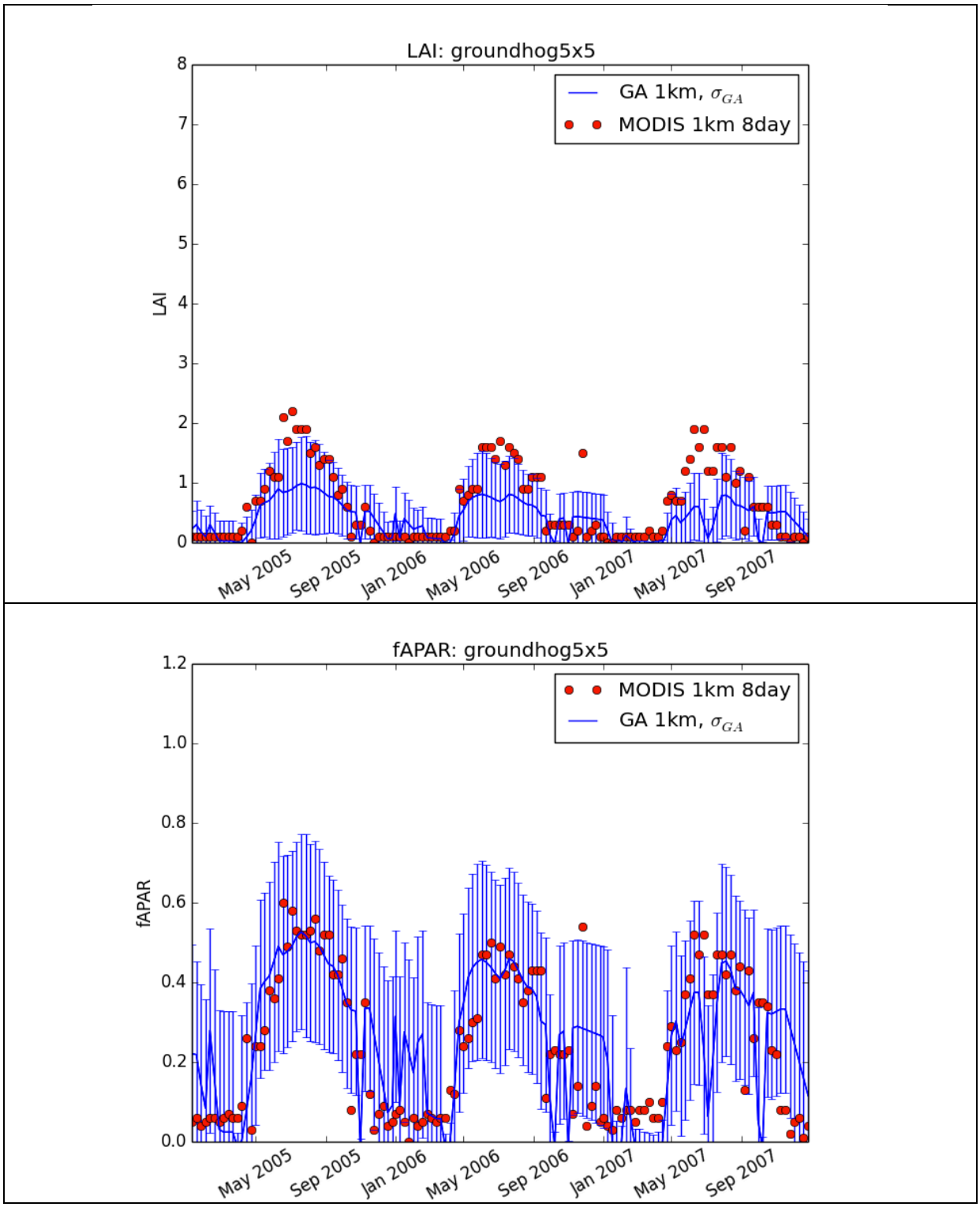

Figure 18 Comparison between JRC-TIP (blue) and MODIS 4 and 8-day (green, red) LAI (top) and fAPAR (bottom) over 2005-2007. Error bars for the TIP are 1 standard deviation of retrievals.

The LAI values for this site are relatively low and agree closely in terms of timing, with the MODIS LAI being around twice that of the TIP LAI in the peak values. The green-up and senescence timing of the signals agree closely, with a steadier increase and decline than some of the other sites seen above. The fAPAR values agree very closely i.e. to within a few % at peak, despite the occasional discrepancy (e.g. January 2006).

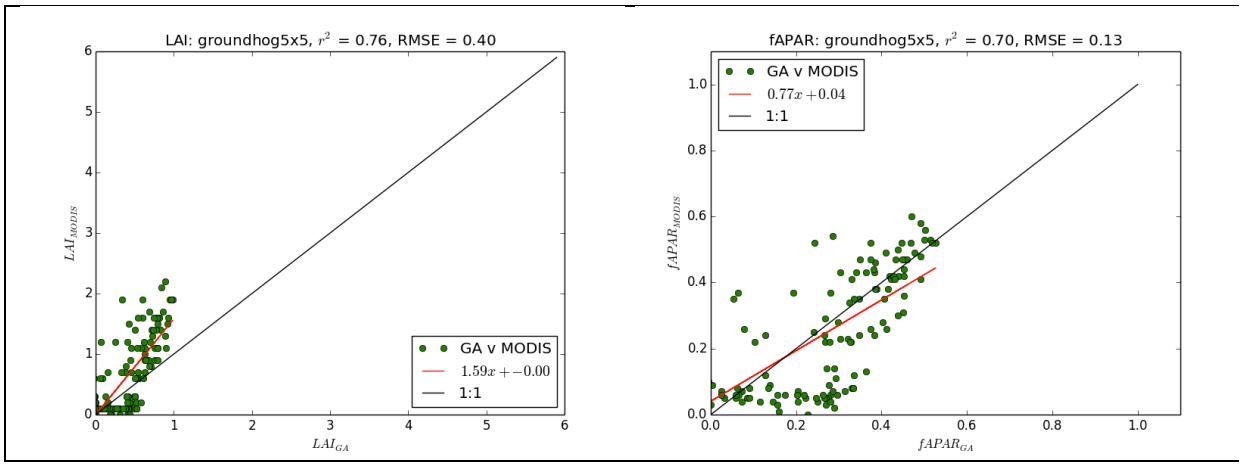

Figure 19 Scatter plots of comparisons shown above.

The r^2 values reflect the relatively good agreement between the TIP and MODIS values. The LAI and fAPAR values have a difference in slope, but with very little offset.

3.2 Regional comparisons

Comparisons are presented here across whole tiles, covering some of the main regions outlined above in the site-level comparisons. TIP and MODIS-derived fAPAR and LAI values are compared for the following tiles:

h18v03: W. Europe including Hainich and Tharandt
h29v12: S. Australia, including Tumbarumba site
h18v07: Central East Africa, including Niger
h09v05: Central USA, including ARM Great Plains site

Tiles are compared from the middle (DAY185) and end (DOY 361) of each year 2005-2007. In each case, the figures show a 2D histogram (or "heatmap") i.e. each point represents the scatter of TIP v MODIS fAPAR or LAI, and the colour represents the frequency of samples at that point. Comparisons are shown first for LAI and then fAPAR for each of the tiles.

It should be noted that the agreement across tiles is likely to be lower than for individual sites, due to the mixed nature of the cover types covered in a given tile. This is particularly true for the mixed tiles, where there is significant agriculture i.e. tile h18v03 for W. Europe. These comparisons are included to show the general trend between the two datasets.

3.2.1 Tile: h18v03

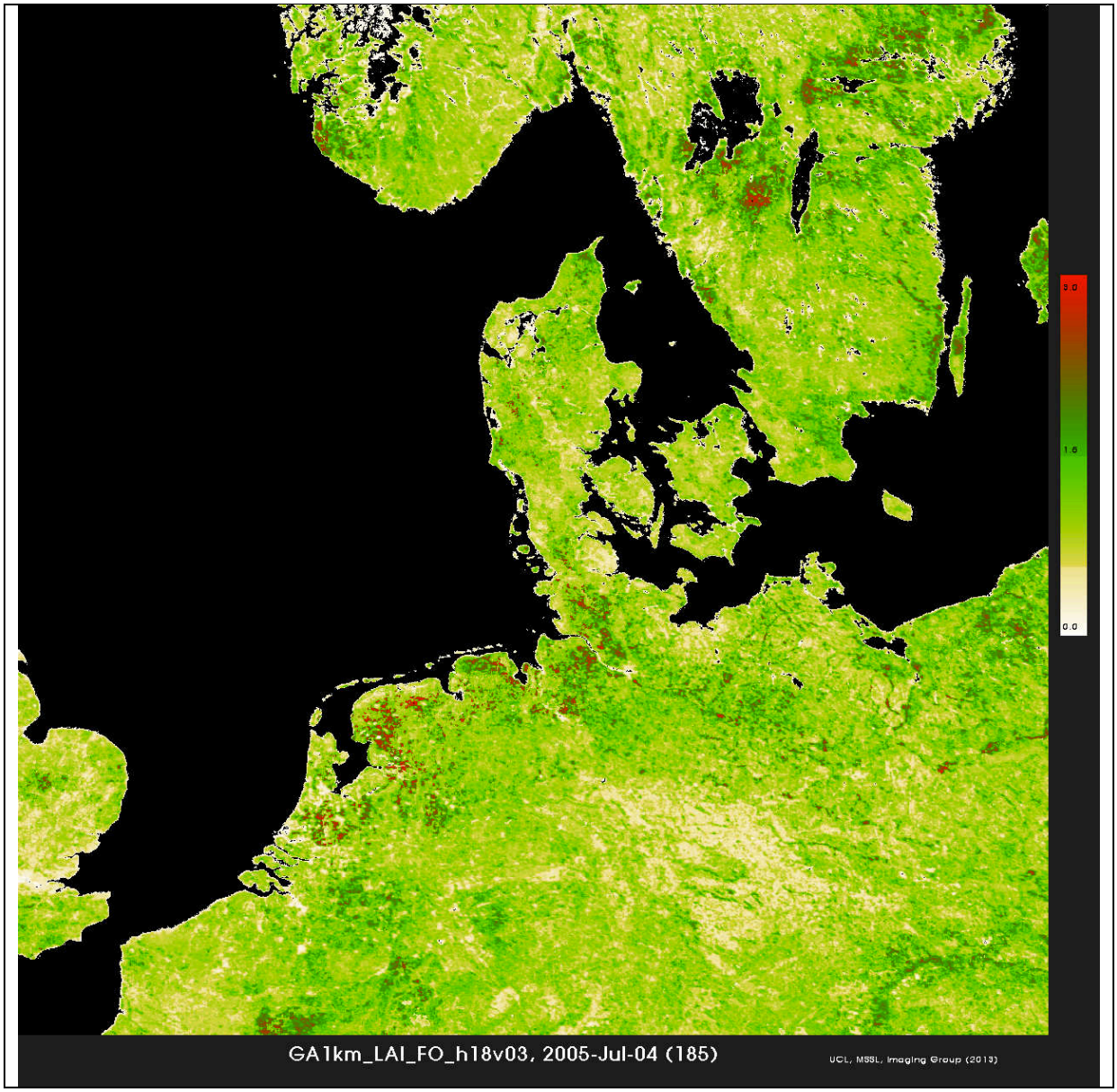

Figure 20 Tile h18v03 LAI for 2005, DOY 185.

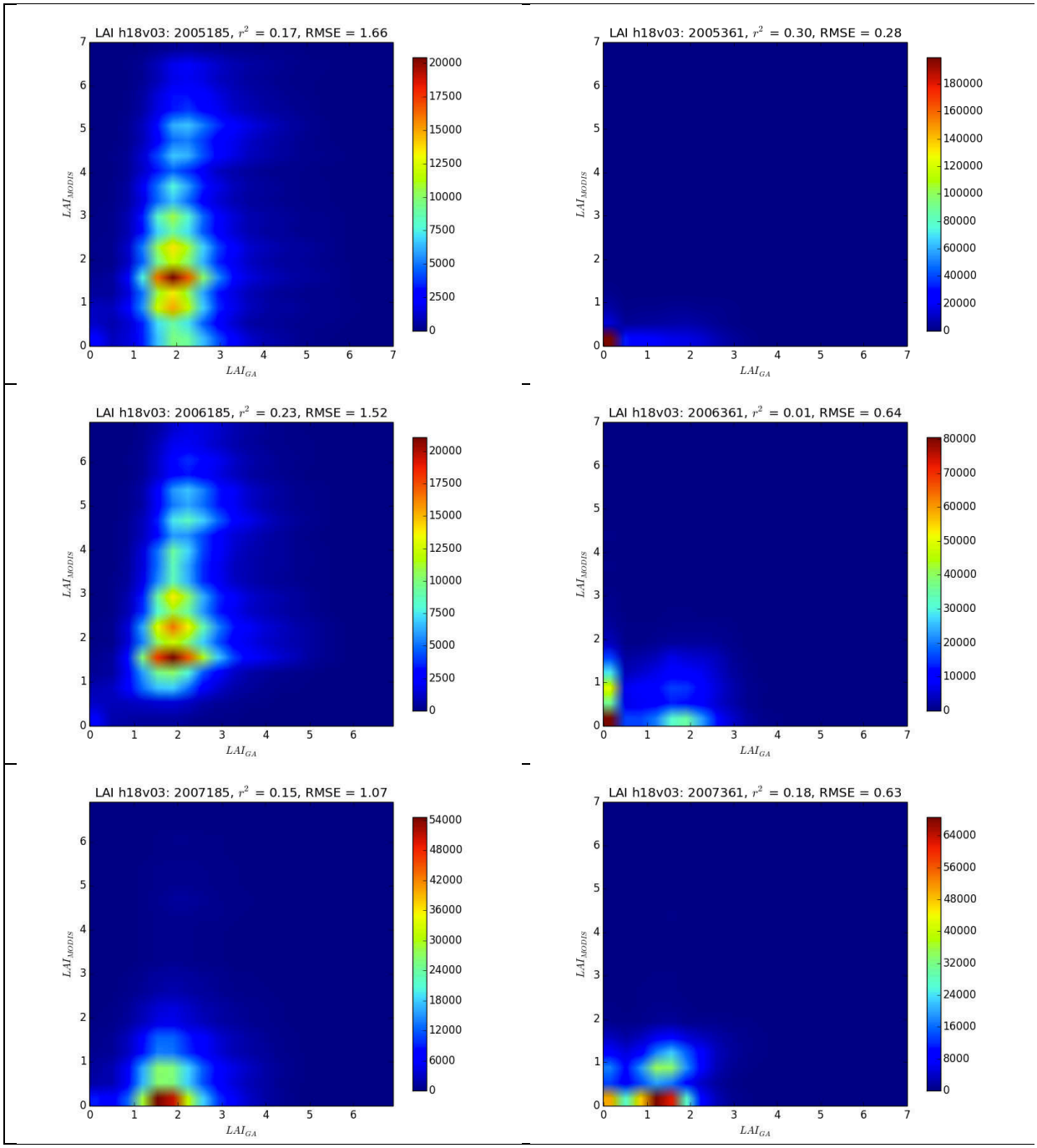

Figure 21 LAI from TIP/GlobAlbedo (horizontal axis) and MODIS (vertical axis) for 2005-2007, top to bottom: 2005-2007. Left (right) column is DOY185 (DOY361).

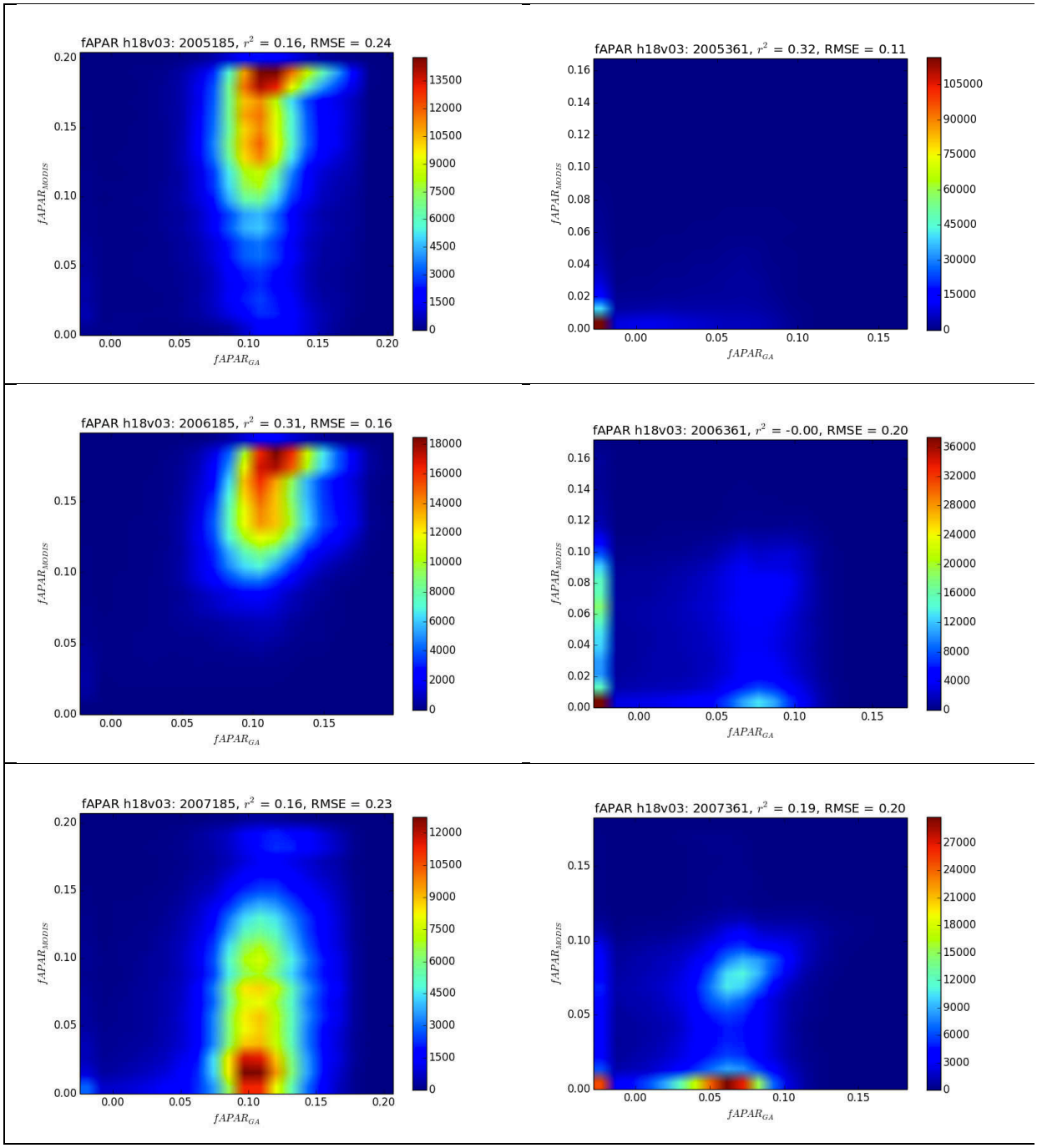

Figure 22 fAPAR from TIP/GlobAlbedo (horizontal axis) and MODIS (vertical axis) for 2005-2007, top to bottom: 2005-2007. Left (right) column is DOY185 (DOY361).

Firstly, in terms of annual trends, we see the expected much higher values of LAI and fAPAR in the middle of the year, and the very low values of both at the ends. Peak values are consistent from year to year, although the values for 2007 are lower than in 2005 and 2006. This is particularly obvious in the MODIS fAPAR which drops considerably in 2007.

It can be seen that for this tile, the agreement between the TIP and MODIS values is quite weak. As discussed above, this is due to the particularly heterogeneous nature of the tile i.e. dominated by agriculture, with large areas of urban, mixed forest etc. The consistently lower values of LAI and fAPAR (and much lower range) in the TIP data, discussed above, are apparent.

3.2.2 Tile: h29v12

Comparisons are shown first for LAI and then fAPAR for each of the tiles.

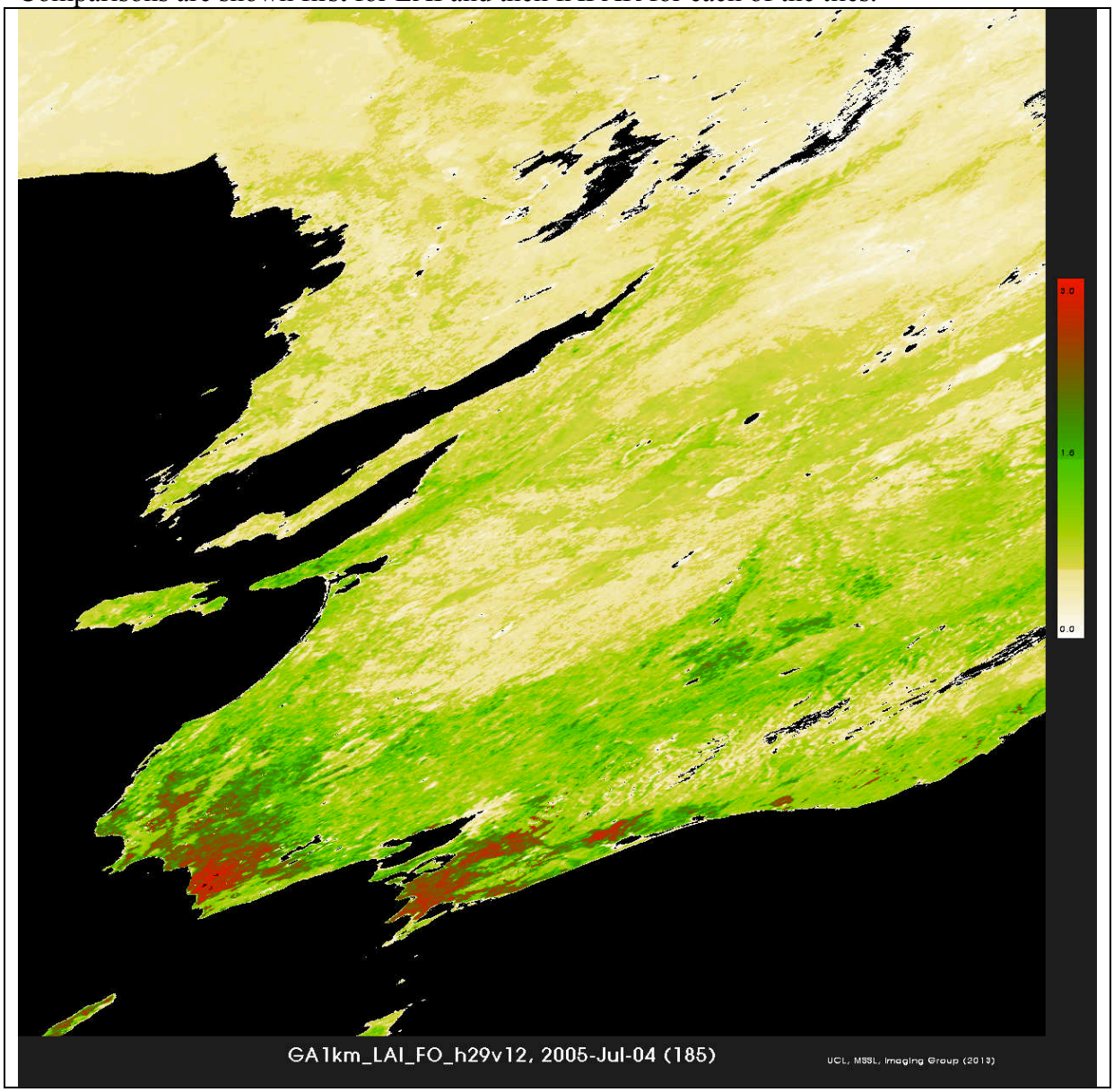

Figure 23 Tile h29v12 LAI for 2005, DOY 185. The severe distortion of the land mass at this distance from the centre of the MODIS SIN projection is apparent. Black and white regions are salt-pans and/or desert regions.

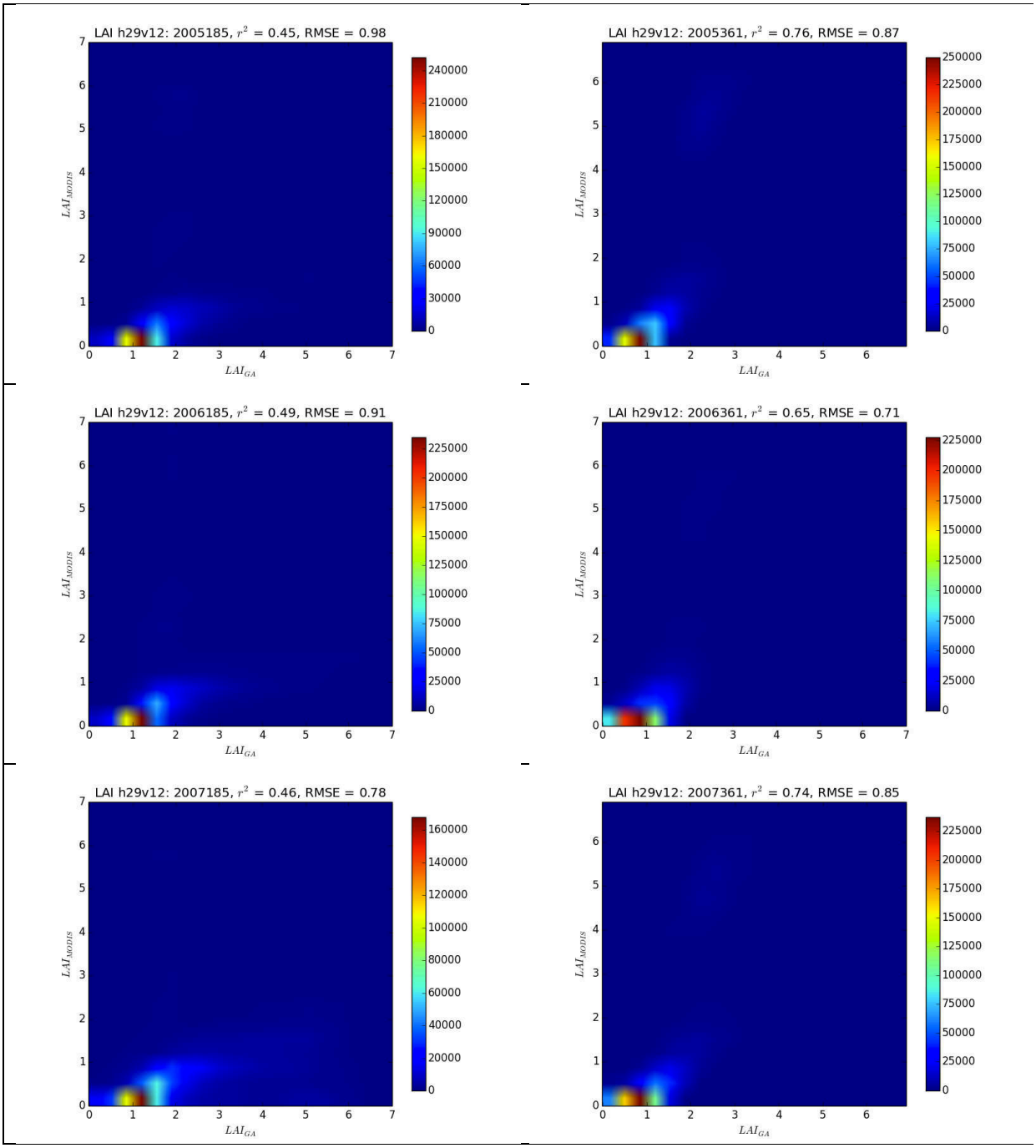

Figure 24 LAI from TIP/GlobAlbedo (horizontal axis) and MODIS (vertical axis) for 2005-2007, top to bottom: 2005-2007. Left (right) column is DOY185 (DOY361).

Clearly, the LAI values at the site are generally low for both datasets, and consistent from year to year. The S. Hemisphere location might suggest that any seasonal variation should be reversed, but given the small variation in general across the tile, this indicates that there is little seasonal variation. There is a much stronger agreement between the TIP and MODIS values at this site, indicative of a more homogeneous cover type.

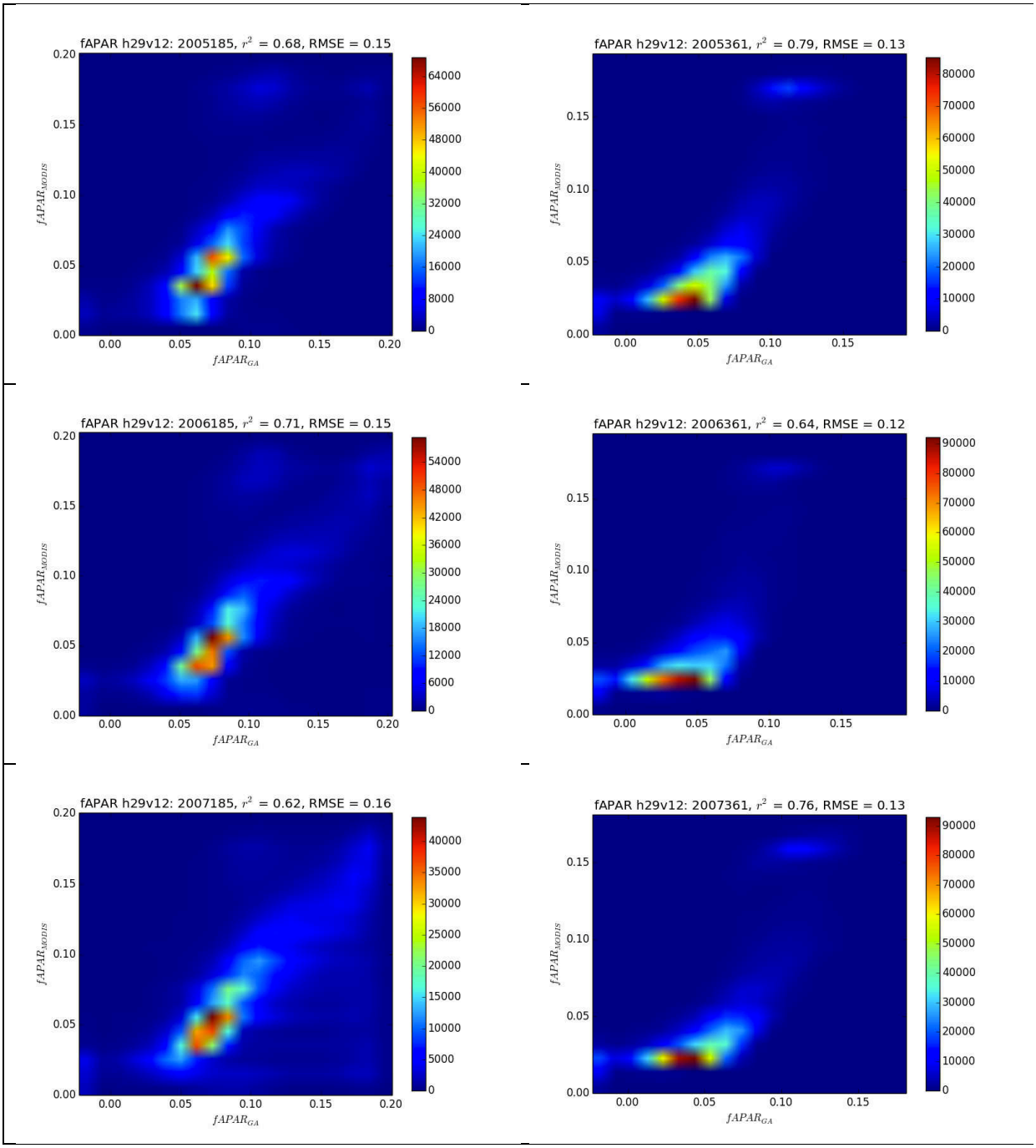

Figure 25 fAPAR from TIP/GlobAlbedo (horizontal axis) and MODIS (vertical axis) for 2005-2007, top to bottom: 2005-2007. Left (right) column is DOY185 (DOY361).

The fAPAR agreement between TIP and MODIS is generally quite strong (r^2 values up to 0.8), with the lower values of TIP apparent across the years.

3.2.3 Tile: h18v07

Comparisons are shown first for LAI and then fAPAR for each of the tiles.

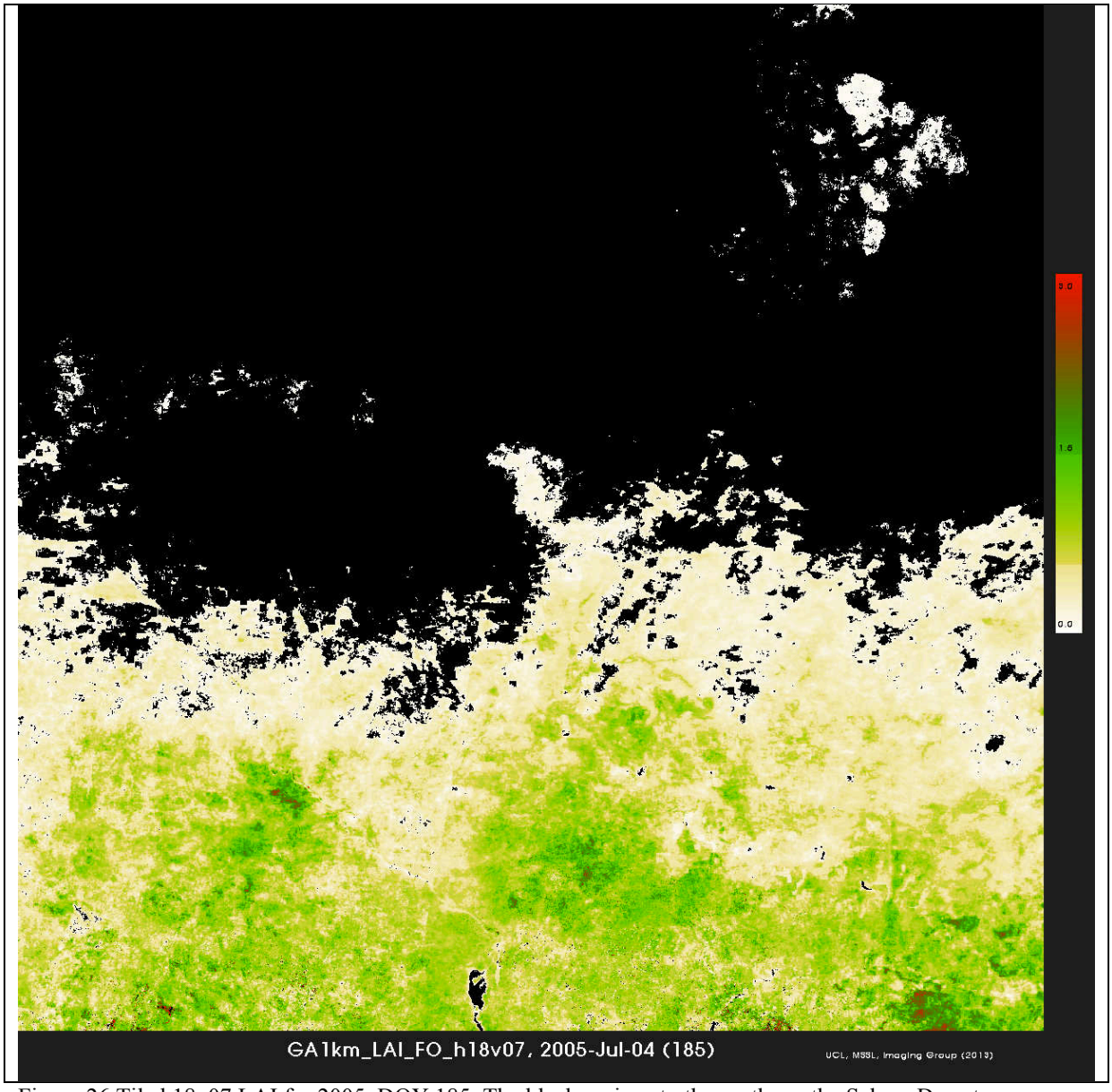

Figure 26 Tile h18v07 LAI for 2005, DOY 185. The black regions to the north are the Sahara Desert.

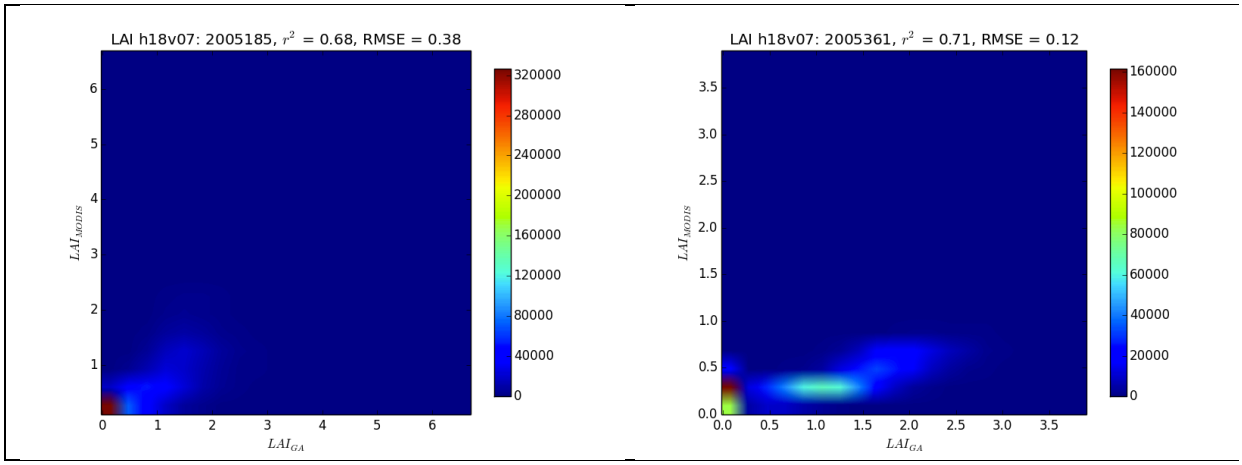

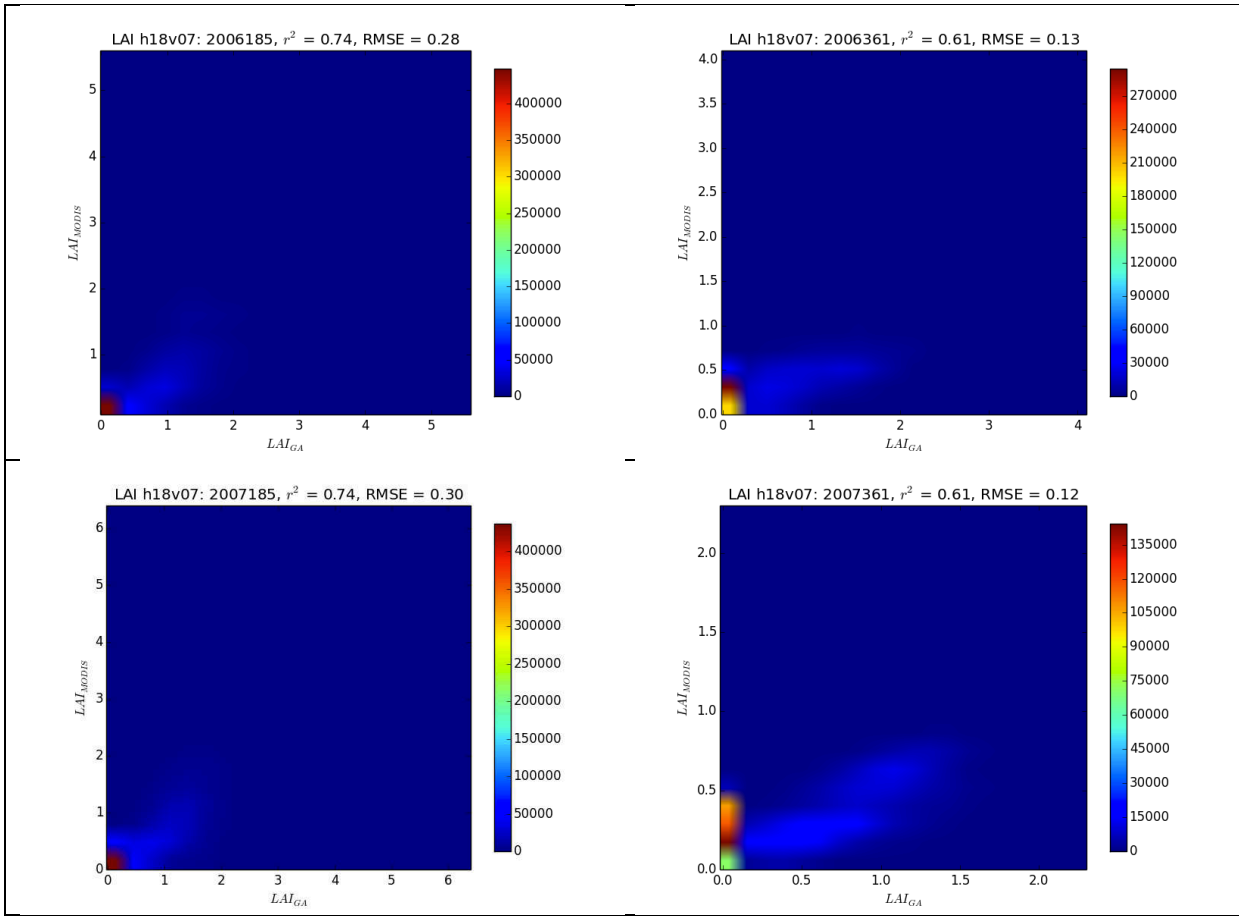

Figure 27 LAI from TIP/GlobAlbedo (horizontal axis) and MODIS (vertical axis) for 2005-2007, top to bottom: 2005-2007. Left (right) column is DOY185 (DOY361).

This tile covers central and W. Africa, including Niger. The LAI values are generally very low in both cases, indicating the sparse grassland and savanna vegetation cover. In terms of seasonal variation, LAI is generally higher towards the end of the year, which is likely to be a response due to rainfall in this essentially tropical equatorial region. Agreement between TIP and MODIS is better for DOY 185 than for DOY 361 but all r^2 are > 0.6.

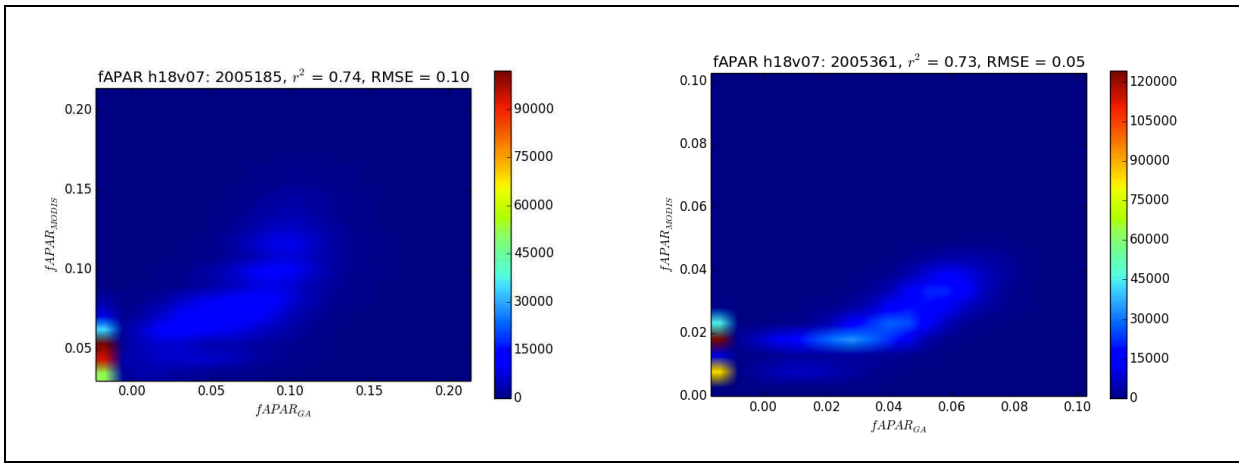

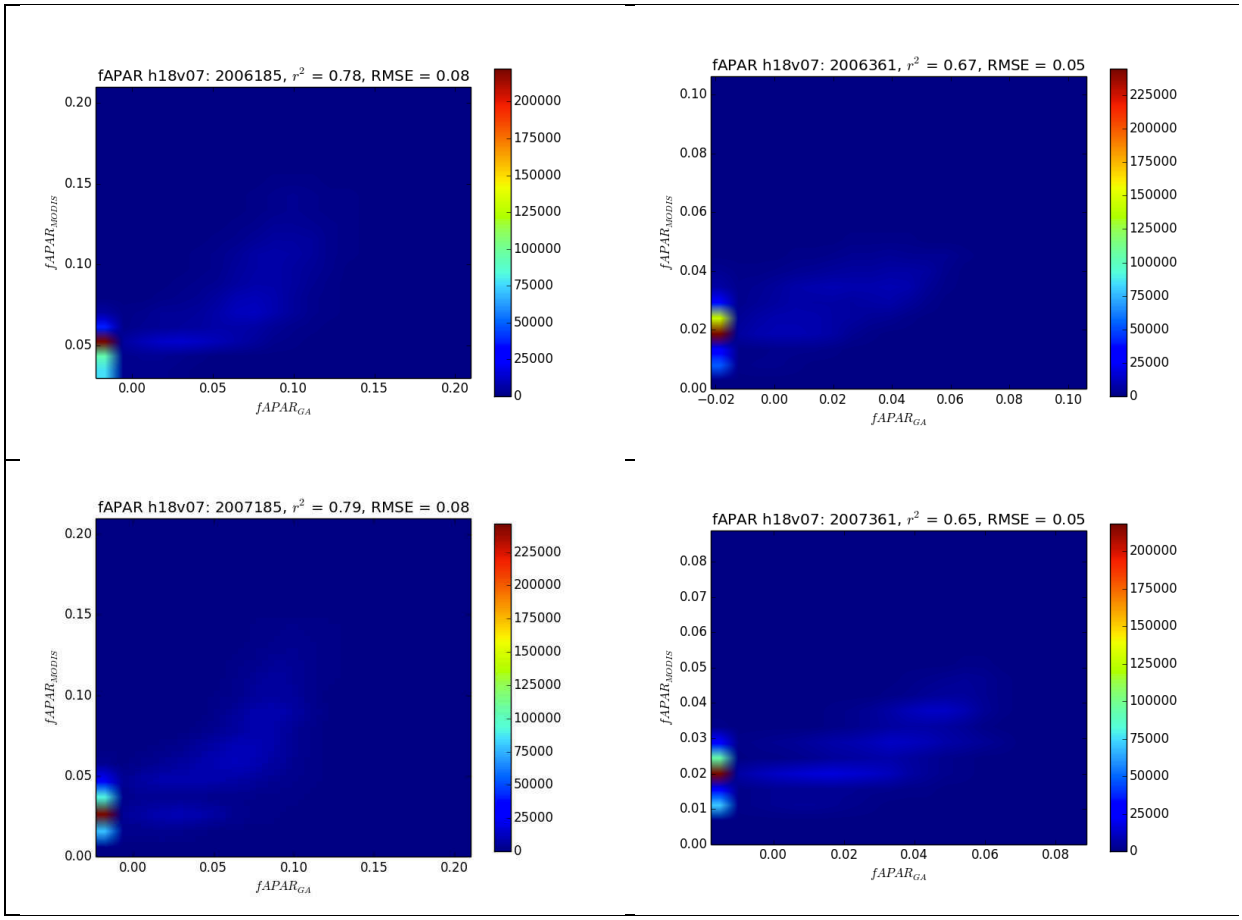

Figure 28 fAPAR from TIP/GlobAlbedo (horizontal axis) and MODIS (vertical axis) for 2005-2007, top to bottom: 2005-2007. Left (right) column is DOY185 (DOY361).

As for the LAI values, fAPAR values are also unsurprisingly quite low, but with a better agreement between TIP and MODIS (all $r^2 > 0.65$).

3.2.4 Tile: h09v05

Comparisons are shown first for LAI and then fAPAR for each of the tiles.

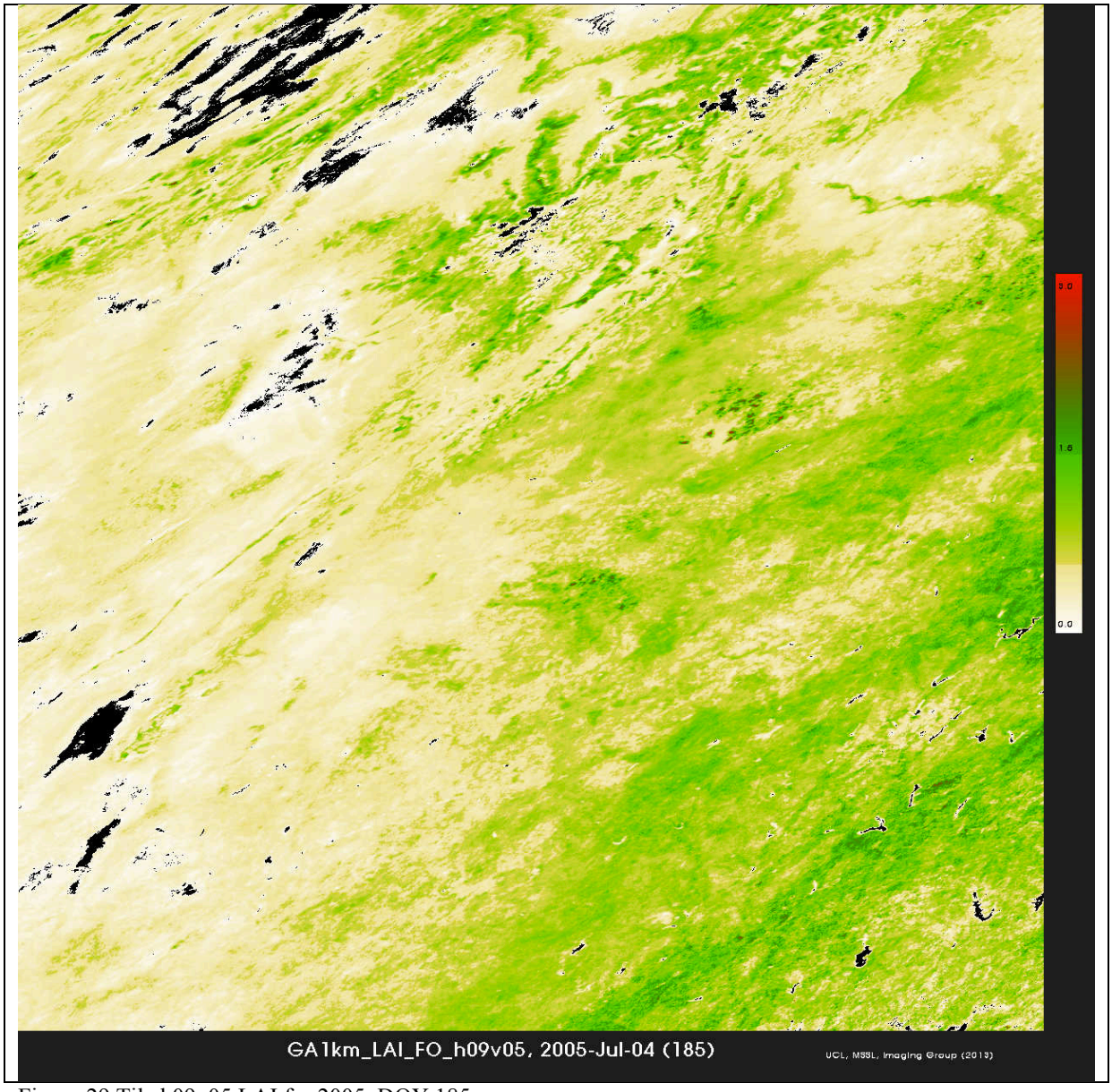

Figure 29 Tile h09v05 LAI for 2005, DOY 185.

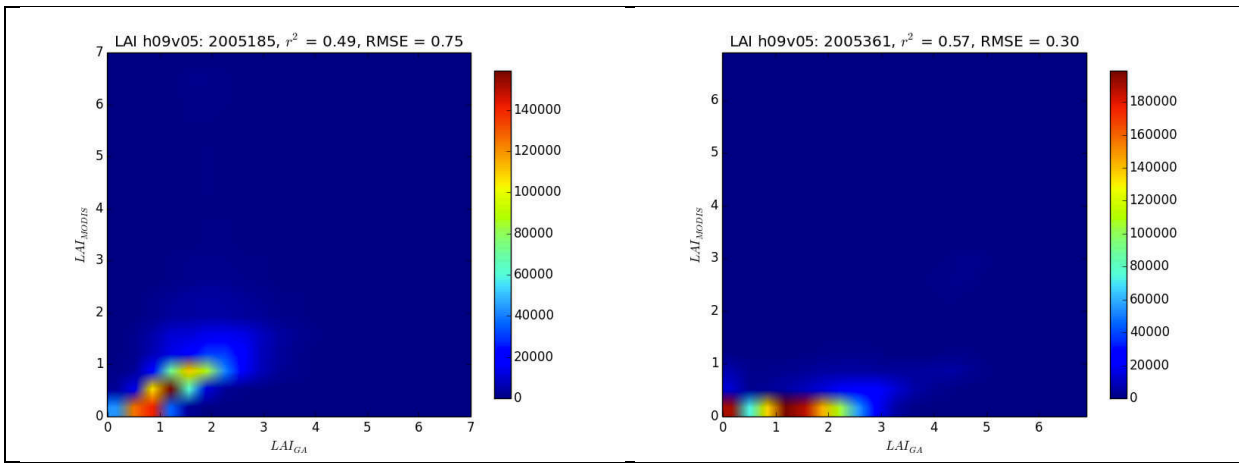

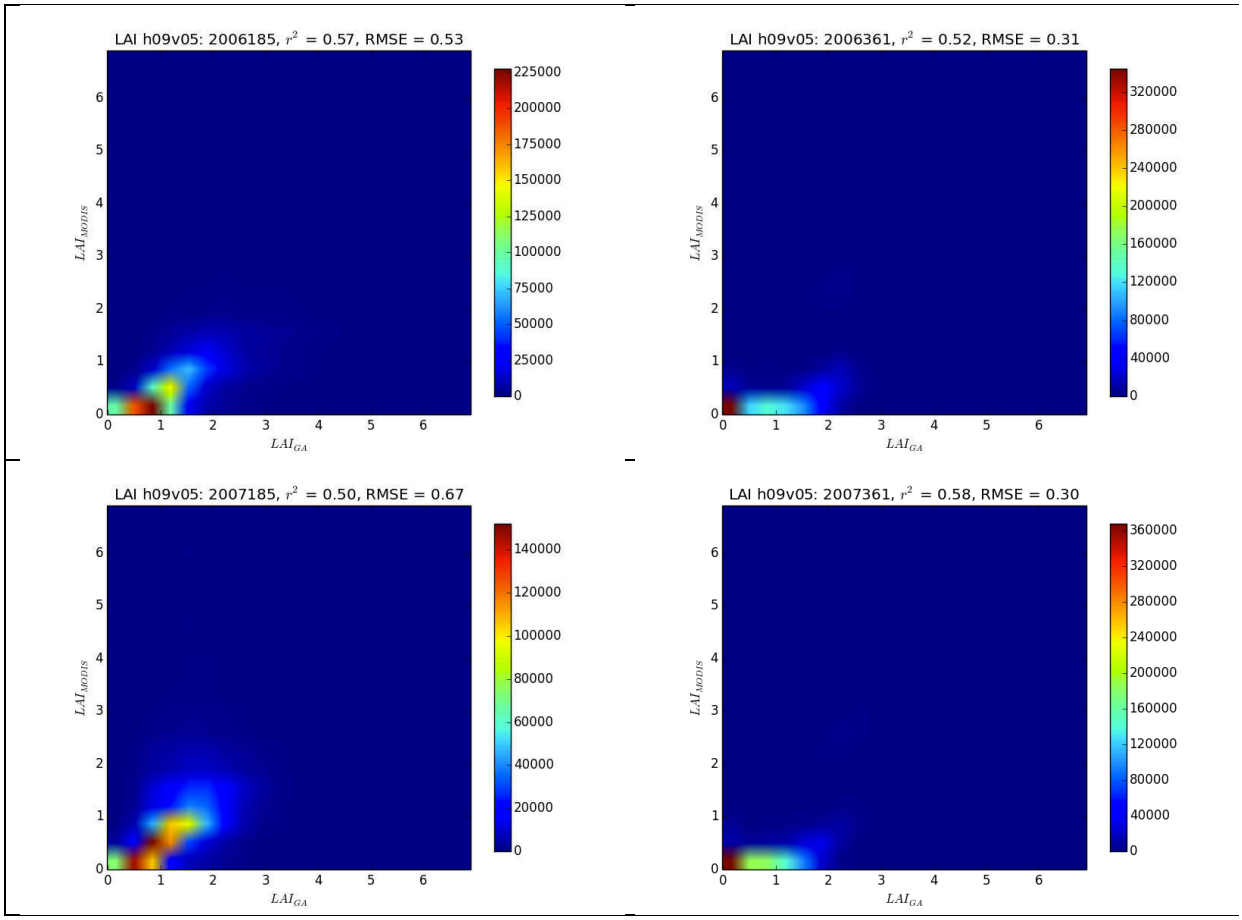

Figure 30 LAI from TIP/GlobAlbedo (horizontal axis) and MODIS (vertical axis) for 2005-2007, top to bottom: 2005-2007. Left (right) column is DOY185 (DOY361).

This tile covers central Southern USA, including the Great Plains ARM site. Again, the relatively sparse, homogenous cover results in a reasonable agreement between the TIP and MODIS LAI values (r^2 >= 0.5). There is clearly a strong seasonal variation in LAI, with much higher values (and range) observed over DOY 185 than for DOY 361 over all years.

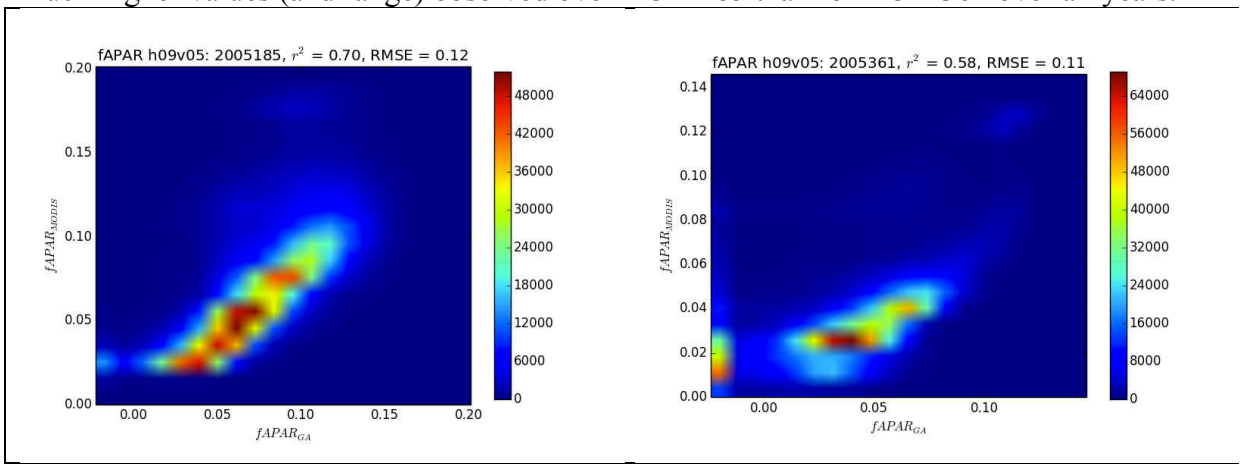

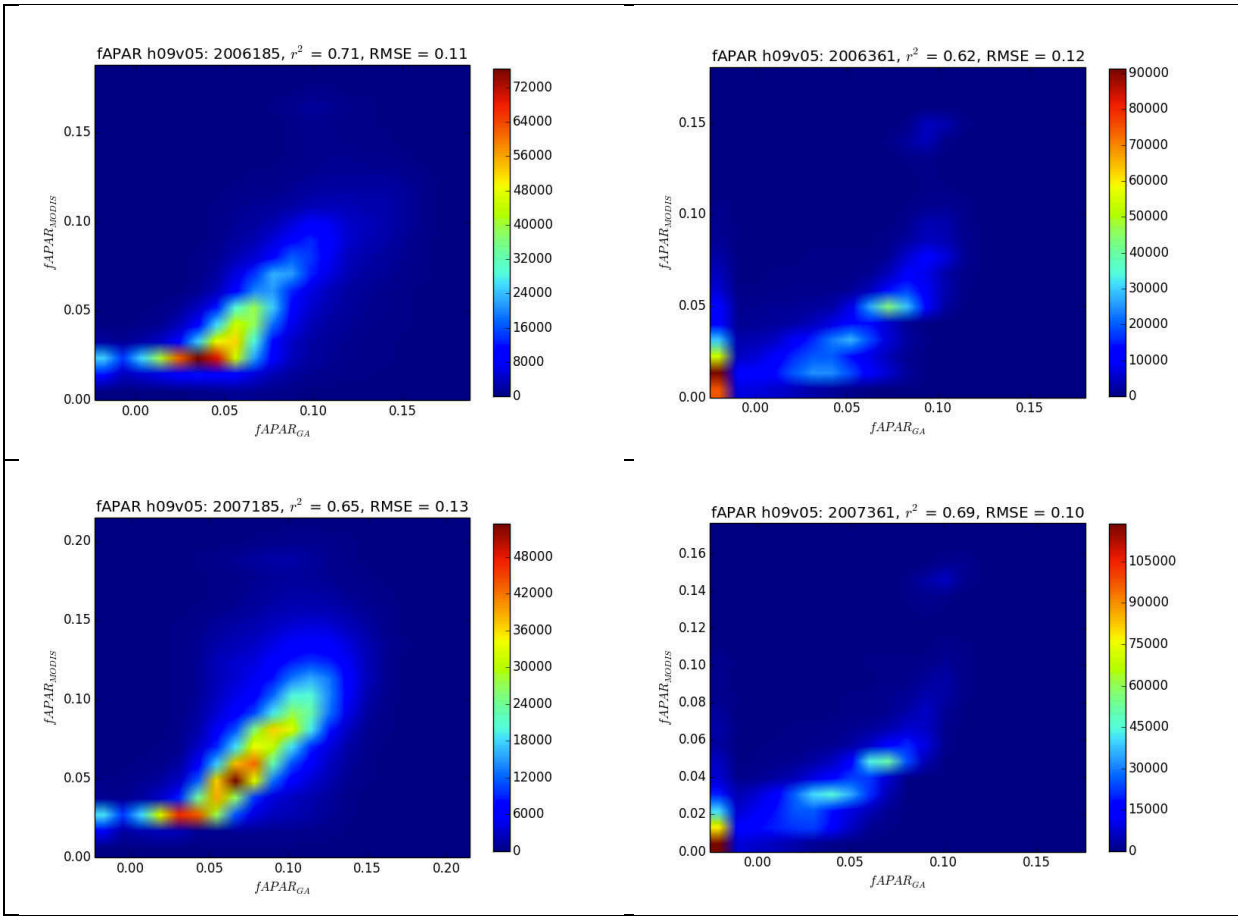

Figure 31 fAPAR from TIP/GlobAlbedo (horizontal axis) and MODIS (vertical axis) for 2005-2007, top to bottom: 2005-2007. Left (right) column is DOY185 (DOY361).

Agreement between TIP and MODIS fAPAR is higher than for LAI, with r^2 of 0.6 or above in all cases. Agreement is higher for the middle of the year, when values are higher as might be expected. The pattern from year to year is similar, albeit with some variation in 2006, showing generally lower values of both TIP and MODIS fAPAR than for 2005 and 2007.

3.3 Whole-hemisphere seasonal comparisons

Below, comparisons are presented between the TIP and MODIS LAI and fAPAR values, on a hemisphere, seasonal basis. All valid land tiles lying in horizontal rows 0-8 on the MODIS tile map, are considered as Northern Hemisphere; all tiles lying in horizontal rows > 8 are considered Southern Hemisphere. All data from DOY185 (NH) and DOY 361 (SH) are considered 'summer'; all data from DOY185 (SH) and DOY 361 (NH) are considered 'winter'. Each tile in each summer/winter case, for each year, are compared by calculating a linear regression between the TIP and MODIS pixel values. The resulting differences between the two are characterised by the slope and intercept of the regression in each case, and the RMSE of the linear model fit, weighted by the number of valid pixels in each tile. These values are collected and shown in (normalised) histograms below. These plots indicate the consistency (or otherwise) of the agreement from season to season and from year to year. They also summarise the overall magnitude of slope and offset between the TIP and MODIS values. In each case, histogram columns are offset by -1/3, 0 and +1/3 for years 2005, 2006,

2007 respectively to make them visible where they overlap significantly; 2006 results are centred on the bin labels.

3.3.1 NH slope, offset and RMSE

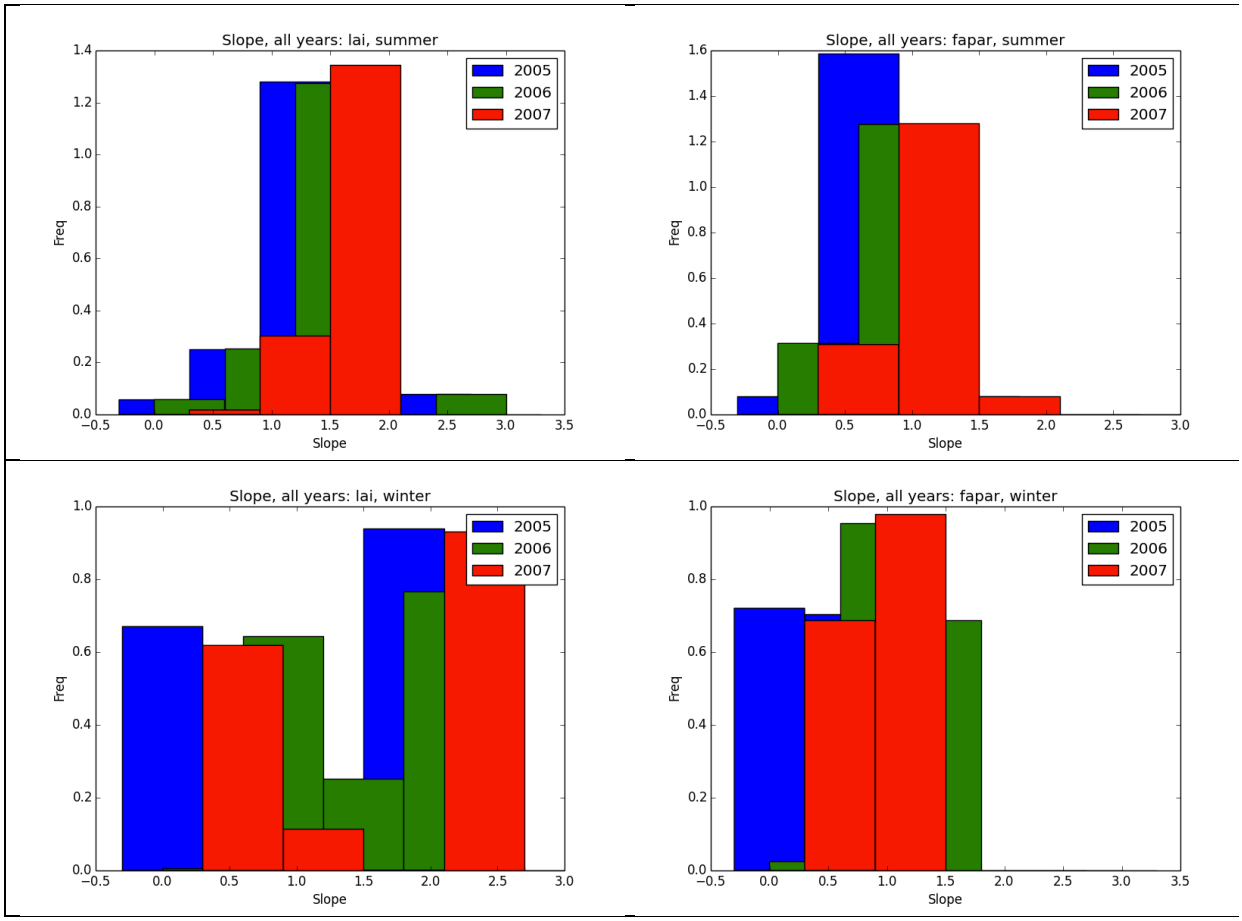

Figure 32 Histograms of the distribution of slope of regression between TIP and MODIS LAI (left column) and fAPAR (right column), for NH summer (top row) and winter (bottom row). Columns are offset with respect to the bin labels for visibility.

These results illustrate that the summer LAI and fAPAR slope is consistent from year-to-year at ~1.6 for LAI and 0.7 for fAPAR. For the winter case, the year to-year variability is greater for LAI particularly; for fAPAR the slope reduces (but of course so does the magnitude).

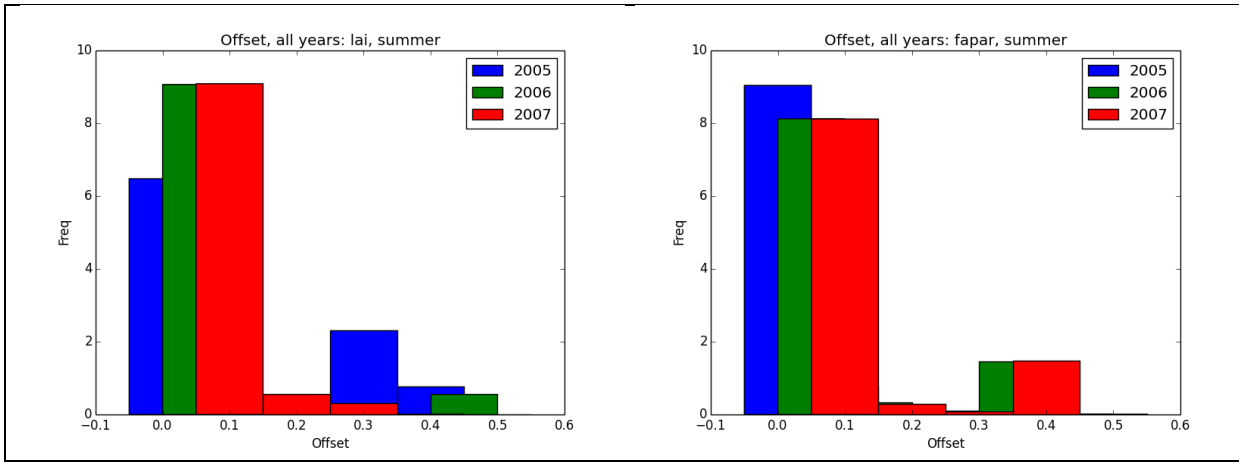

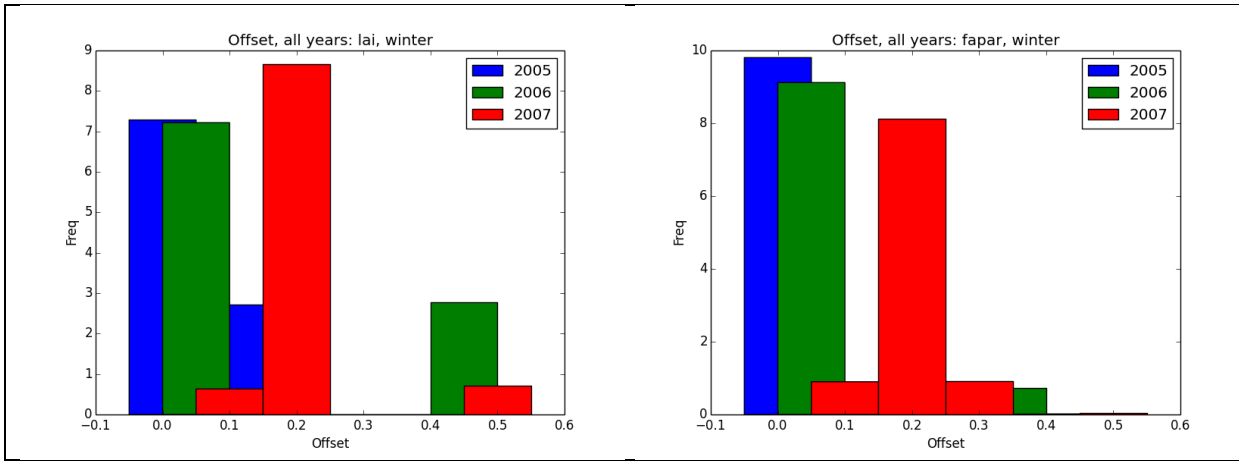

Figure 33 Histograms of the distribution of offset (intercept) of regression between TIP and MODIS LAI (left column) and fAPAR (right column), for NH summer (top row) and winter (bottom row). Columns are offset with respect to the bin labels for visibility.

The histograms of the offsets show that for both LAI and fAPAR, the offset is consistent from year-to-year in the summer at around 0.05 for both. In the NH winter case, the offset is both higher and more variable, with differences year-to-year, particularly between 2005-6 and 2007, where the offset in both LAI and fAPAR is increased.

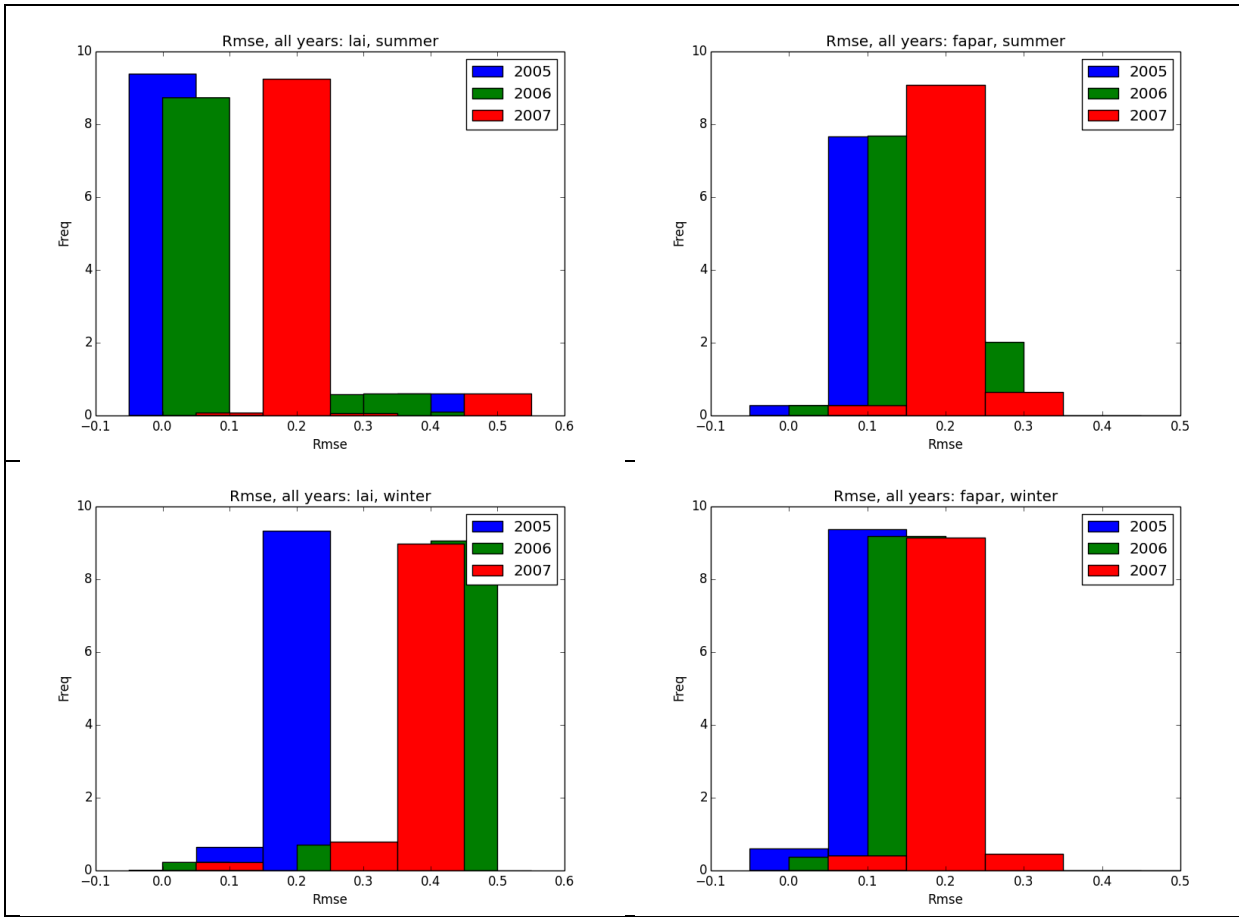

Figure 34 Histograms of the distribution of RMSE values for regression fit between TIP and MODIS LAI (left column) and fAPAR (right column), for NH summer (top row) and winter (bottom row). Columns are offset with respect to the bin labels for visibility.

The RMSE of model fit is significantly higher for LAI in 2007 NH summer, than the previous two years; RMSE for fAPAR is consistent from year-to-year at 0.2 for NH summer. For the winter case, the year to-year variability is greater for LAI particularly; for fAPAR the RMSE is very similar to the summer case.

3.3.2 SH slope, offset and RMSE

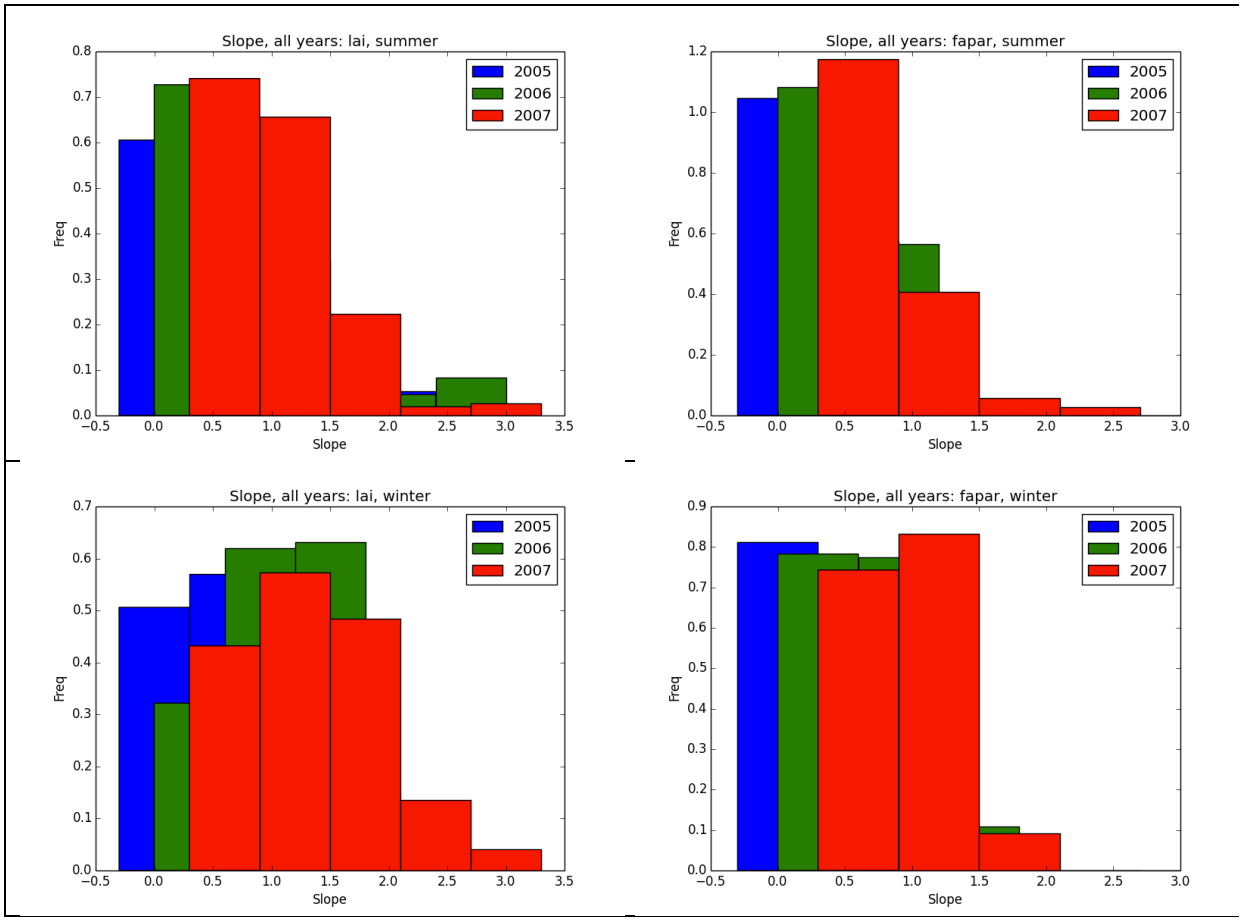

Figure 35 Histograms of the distribution of slope of regression between TIP and MODIS LAI (left column) and fAPAR (right column), for SH summer (top row) and winter (bottom row). Columns are offset with respect to the bin labels for visibility.

These results illustrate that the summer LAI and fAPAR slope is more variable from year-to-year than for the SH cases above. For LAI the slope is slightly lower, particularly for 2006 at 0.5, and ~1.6 for 2005 and 2007. For fAPAR, values are generally around 0.5 in the summer. For the winter case, the year to-year variability is greater for LAI particularly, and the slope higher at between 1 and 2; for fAPAR the slope is somewhat higher than the summer case, and broadly consistent from year-to-year at 0.5-1.5.

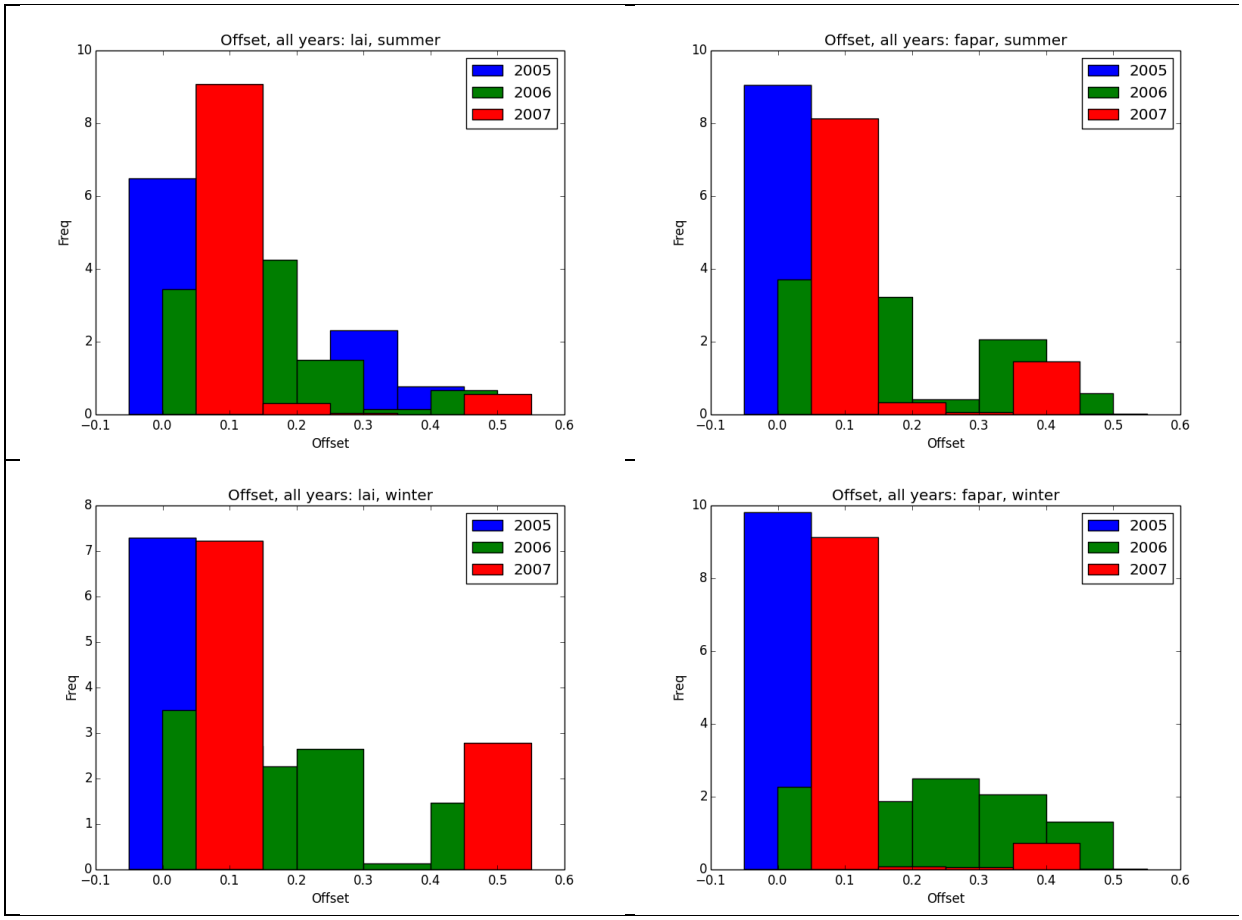

Figure 36 Histograms of the distribution of offset (intercept) of regression between TIP and MODIS LAI (left column) and fAPAR (right column), for SH summer (top row) and winter (bottom row). Columns are offset with respect to the bin labels for visibility.

The histograms of the offsets show that for both LAI and fAPAR, the offset is consistent from year-to-year in the summer at around 0.1 for both, skewed to the lower values. In the SH winter case, the offset is both higher and more variable, with differences year-to-year, particularly 2006, where the offset in both LAI and fAPAR is spread across a wider range of values up to 0.5.

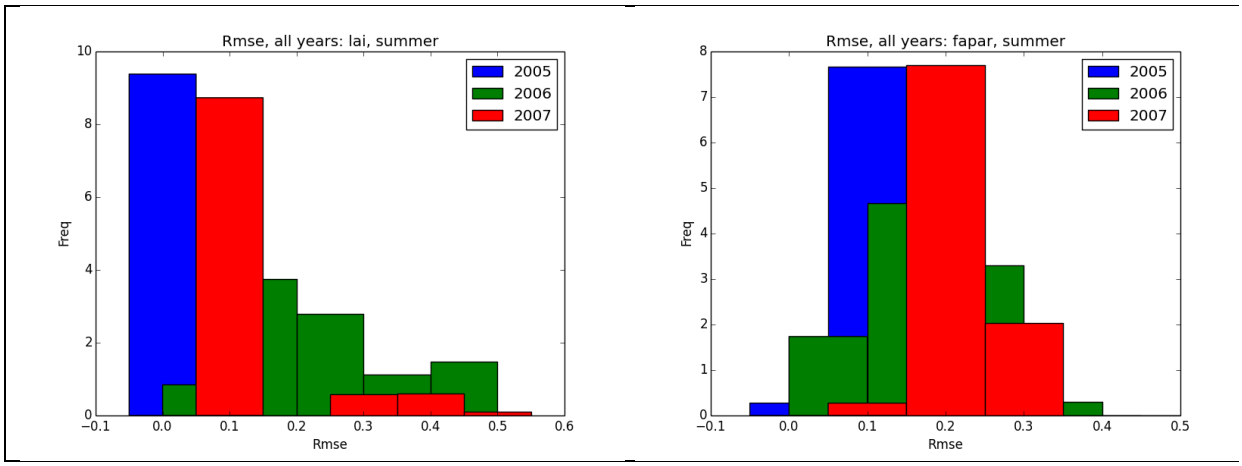

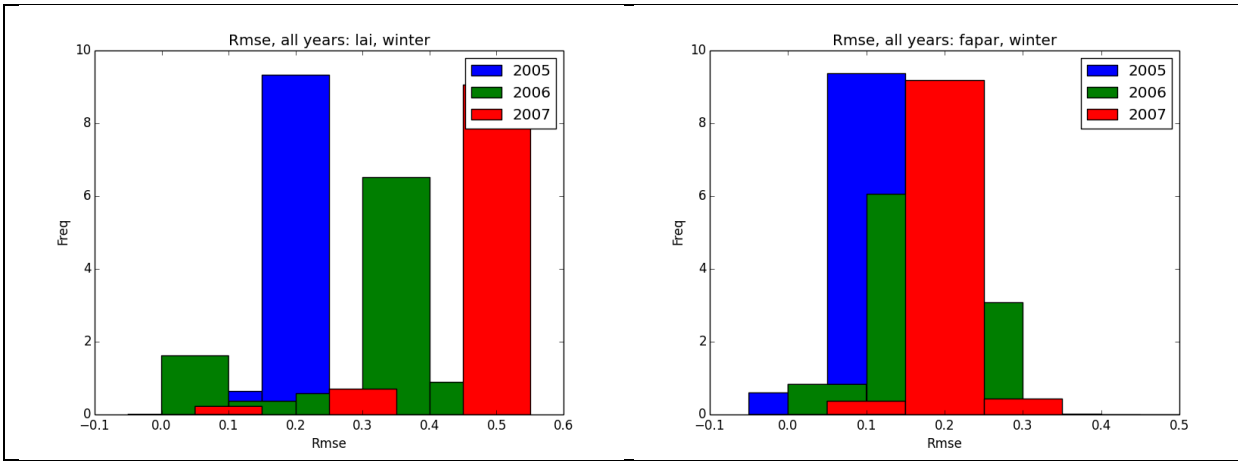

Figure 37 Histograms of the distribution of RMSE values for regression fit between TIP and MODIS LAI (left column) and fAPAR (right column), for NH summer (top row) and winter (bottom row). Columns are offset with respect to the bin labels for visibility.

The RMSE of model fit is consistent from year-to-year for LAI in 2007 SH summer, at ~0.1, albeit with greater variability in 2006. The distribution of RMSE for fAPAR is consistent from year-to-year at 0.2 for SH summer. For the SH winter cases, RMSE for LAI comparison is higher than for the summer cases, and more variable from year-to-year. For fAPAR there is little difference between summer and winter, or from year to year. Distribution of RMSE for fAPAR is very consistent between NH and SH for both summer and winter.

4 Summary

Values of LAI and fAPAR have been compared from the TIP algorithm, based on the GlobAlbedo data, and the MODIS algorithm, derived from MODIS reflectance data. As noted above, these two sets of products are based on different assumptions: in the case of the TIP-derived values, this is a 1D radiative transfer scheme designed to be consistent with the observations used to drive it. This results in values of LAI and fAPAR that are consistent, radiometrically in both observations and RT model inversion scheme, but are then effective values i.e. values consistent with a 1D approximation to a 3D RT problem, where clumping is not accounted for. The MODIS products are generated using a 3D RT scheme, and thus LAI values are 'real' in as much as they represent the LAI within this 3D scheme. However these values are still not real in as much as they are derived from large scale (250m to 1km) observations assuming cover is homogeneous within each pixel.

A key point to note in the comparison between TIP and MODIS products is the temporal consistency across each year. At a given site, and even averaged over several pixels, the variance of the MODIS values is large – varying by factors of up to 6 or 7 at times over the space of 8 days. This is largely due to the influence of residual cloud and snow contamination that causes rapid fluctuations due to poor quality retrievals, even through they may not be flagged as such. The GlobAlbedo data are based on a moving window approach, which generates a model-based prediction of the surface reflectance properties with a prior expectation. This is very much more robust to outliers, which is obvious in the temporal profiles. This is likely to provide a more conservative estimate, temporally, than from MODIS, which over larger scales (tiles to regions) ought to prove more robust temporally.

In general, this difference in terms of the model inversion approaches leads to consistently lower values of LAI and fAPAR in the TIP-derived products compared to MODIS. From the individual site comparisons the slope of the relationship between TIP and MODIS LAI across three years ranges from 1.1 to 2.9, mean = 1.9, σ = 0.48. For fAPAR, the difference is smaller, ranging from 0.5 to 1.07, mean = 0.85, σ = 0.2. The offset in LAI varies from 0.12 to 1, mean = 0.47, σ = 0.36. The offset in fAPAR varies from 0.12 to 0.47, mean = 0.23, σ = 0.13. Note that these are based on individual site comparisons.

These differences and offsets are shown to be quite stable, for the whole hemisphere comparisons, between NH and SH. However, the variation in slope and offset is larger for winter than summer cases, which reflects the generally lower values of both, and more importantly, the reduced quality and frequency of observations. Globally, the comparisons show: slope of the relationship between TIP and MODIS LAI across three years mean = 1.55, σ = 0.2; offset mean = 0.21, σ = 0.45 For fAPAR, slope mean = 0.76, σ = 0.20; offset mean = 0.08, σ = 0.09.

The recommendation we would make is that if users require a calibration between TIP-derived LAI and fAPAR products against those derived from different RT approaches and assumptions, particularly for a given site, they can calculate a site-based or tile-based local calibration using the GlobAlbedo tool: http://www.globalbedo.org/point_faparlai.php

5 Acknowledgements

The authors would like to thank ESA for their support through Estellus. FastOpt did the processing of all TIP products on a pro bono basis. The fapar/LAI GUI and subsetting tool was developed with NCEO funding at UCL-MSSL by Dr Said Kharbouche.

6 References cited

Bojinski, S., Verstraete, M. M., Peterson, T. C., Simmons, A. and Zemp, M. (2014, in press) The concept of Essential Climate Variables in support of climate research, applications, and policy, Bulletin of the American Meteorological Society, 10.1175/BAMS-D-13-00047.1.

Ceccherini, G., Gobron, N. and Robustelli, M. (2013) Harmonization of Fraction of Absorbed Photosynthetically Active Radiation (FAPAR) from Sea-Viewing Wide Field-of-View Sensor (SeaWiFS) and Medium Resolution Imaging Spectrometer Instrument (MERIS), Remote Sensong, 5, 3357-3376, doi:10.3390/rs5073357.

Chen, J. M. & Black, T. A. (1992) Defining leaf area index for non-flat leaves, Plant, Cell and Environment, 15, 421–429.

Chen, J. M., Menges, C. H. & Leblanc, S. (2005) Global derivation of the vegetation clumping index from multi-angular satellite data, Remote Sensing of Environment, 97, 447–457.

Globalbedo Algorithm Theoretical Basis Document (ATBD) http://www.globalbedo.org/docs/GlobAlbedo_Albedo_ATBD_V4.12.pdf (accessed 27/1/2014).

Jelinsky, D. E. and Wu, J. (1996) The modifiable areal unit problem and implications for landscape ecology, *Landscape Ecology*, **11(3)**, 129-140.

Jonckheere, I., Fleck, S., Nackaerts, K., Muys, B., Coppin, P., Weiss, M. and Baret, F. (2004) Methods for leaf area index determination part I: theories, techniques and instruments, Agricultural Forest Meteorology, 121, 19-35.

Knyazikhin, Y., Martonchik, J. V., Myneni, R. B., Diner, D. J. and Running, S. W. (1998) Synergistic algorithm for estimating vegetation canopy leaf area index and fraction of absorbed photosynthetically active radiation from MODIS and MISR data, J. Geophys. Res., 103, 32257 – 32274.

Knyazikhin, Y., J. Glassy, J. L. Privette, Y. Tian, A. Lotsch, Y. Zhang, Y. Wang, J. T. Morisette, P.Votava, R.B. Myneni, R. R. Nemani, S. W. Running (1999) MODIS Leaf Area Index (LAI) and Fraction of Photosynthetically Active Radiation Absorbed by Vegetation (FPAR) Product (MOD15), Algorithm Theoretical Basis Document (ATBD), http://eospso.gsfc.nasa.gov/atbd/modistables.html.

Liang, S. (2000) Numerical experiments on spatial scaling of land surface albedo and leaf area index, *Remote Sensing Reviews*, **19**, 225-242.

Liang, S. (2004) Quantitative Remote Sensing of Land Surfaces, John Wiley and Sons, Inc., New Jersey, ISBN 0-471-28166-2.

Pfeifer, M. Disney, M. I., Quaife, T., and Marchant, R. (2012) Terrestrial ecosystems from space: a review of earth observation products for macroecology applications *Glob. Ecol. and Biogeog.*, 21, 603-624, DOI: 10.1111/j.1466-8238.2011.00712.x.

Pinty B., Lavergne T., Dickinson R. E., Widlowski J.-L., Gobron N. and Verstraete M. M. (2006) Simplifying the Interaction of Land Surfaces with Radiation for Relating Remote Sensing Products to Climate Models, Journal of Geophysical Research Atmospheres, 111(2).

Pinty, B., T. Lavergne, M. Voßbeck, T. Kaminski, O. Aussedat, R. Giering, N. Gobron, M. Taberner, M. M. Verstraete, and J.-L. Widlowski (2007) Retrieving surface parameters for climate models from MODIS and MISR albedo products, J. Geophys. Res., 112, D10116, doi:10.1029/ 2006JD008105.

Pinty, B., Jung, M., Kaminski, T., Lavergne, T., Mund, M., Plummer, S., Thomas, E., Widlowski, J.L. (2011) Evaluation of the JRC-TIP 0.01° products over a mid-latitude deciduous forest site. Remote Sens. Environ. 115, 3567-3581.

Pinty, B., Andredakis, I., Clerici, M., Kaminski, T., Taberner, M., Verstraete, M. M., et al. (2010a) Exploiting the MODIS albedos with the Two-stream Inversion Package (JRC-TIP) Part I: effective Leaf Area Index, Vegetation and Soil properties. Journal of Geophysical Research, 116.

Pinty, B., Clerici, M., Andredakis, I., Kaminski, T., Taberner, M., Verstraete, M. M., et al. (2010b) Exploiting the MODIS albedos with the Two-stream Inversion Package JRC-TIP) Part II: Fractions of transmitted and absorbed fluxes in the vegetation and soil layers. Journal of Geophysical Research, 116, D09106, doi:10.1029/2010JD015373.

Pfeifer, M., Disney, M. I., Quaife, T. and Marchant, R. (2012) Terrestrial ecosystems from space: a review of earth observation products for macroecology applications, Global Ecology and Biogeography, 21, 603–624.

Running, S. W., Nemani, R., Glass, J. M. and Thornton, P. E. (1999) MODIS daily photosynthesis (PSN) and annual net primary production (NPP) product (MOD17): Algorithm Theoretical Basis Document (ATBD), http://modis.gsfc.nasa.gov/data/atbd/atbd_mod16.pdf.

Voßbeck, M., M. Clerici, T. Kaminski, B. Pinty, T. Lavergne, and R. Giering (2010) An inverse radiative transfer model of the vegetation canopy based on automatic differentiation. Inverse Problems, 26(9), 2010.

Voßbeck, M., R. Giering, and T. Kaminski. Development and First Applications of TAC++. In C. Bischof, H. M. Bücker, P. D. Hovland, U. Naumann, and J. Utke, editors (2008) Advances in Automatic Differentiation, Lecture Notes in Computational Science and Engineering, pages 187-197, Berlin, 2008, Springer.

Weiss, M., Baret, F., Smith, G. J., & Jonckheere, I. (2004) Methods for in situ leaf area index measurement, part II: From gap fraction to leaf area index: Retrieval methods and sampling strategies. *Agricultural and Forest Meteorology*, 121, 17-53.

Widlowski, JL, Pinty, B, Clerici, M, Dai, Y. De Kauwe, M, de Ridder, K, Kallel, A, Kobayashi, H, Lavergne, T, Ni-Meister, W, Olchev, A, Quaife, T, Wang, S, Yang, W, Yang, Y and Yuan, H (2011) RAMI4PILPS: An intercomparison of formulations for the partitioning of solar radiation in land surface models. Journal of Geophysical Research, 116, G02019, 25.